CONF-880613--26

DE89 004798

VOID FORMATION AND HELIUM EFFECTS IN 9Cr-1MoVNb AND 12Cr-1MoVW STEELS IRRADIATED IN HFIR AND FFTF AT 400°C

P.J. Maziasz and R.L. Klueh

Metals and Ceramics Division, Oak Ridge
National Laboratory, Oak Ridge, TN 37831

ABSTRACT: Martensitic/ferritic 9Cr-1MoVNb and 12Cr-1MoVW steels doped with up to 2 wt% Ni have up to 450 appm He after HFIR irradiation to ~38 dpa, but only 5 appm He after 47 dpa in FFTF. No fine He bubbles and few or no larger voids were observable in any of these steels after FFTF irradiation at 407°C. By contrast, many voids were found in the undoped steels (30-90 appm He) irradiated in HFIR at 400°C, while voids plus many more fine He bubbles were found in the Ni-doped steels (400-450 appm He). Irradiation in both reactors at ~400°C produced significant changes in the as-tempered lath/subgrain boundary, dislocation, and precipitation structures that were sensitive to alloy composition, including doping with Ni. However, for each specific alloy the irradiation-produced changes were exactly the same comparing samples irradiated in FFTF and HFIR, particularly the Ni-doped steels. Therefore, the increased void formation appears solely due to the increased helium generation found in HFIR. While the levels of void swelling are relatively low after 37-39 dpa in HFIR (0.1-0.4%), details of the microstructural evolution suggest that void nucleation is still progressing, and swelling could increase with dose. The effect of helium on void swelling remains a valid concern for fusion application that requires higher dose experiments.

KEY WORDS: Martensitic/ferritic steels, helium, Ni-doping, voids, bubbles, precipitation, $M_{23}C_6$, M_6C, MC, lath/subgrain boundary structure, neutron irradiation, fusion

DISCLAIMER

*Research sponsored by the Office of Fusion Energy, U.S. Department of Energy, under Contract No. DE-AC05-84OR21400 with the Martin Marietta Energy Systems, Inc.

INTRODUCTION

Martensitic/ferritic steels are attractive candidate structural first wall materials for magnetic fusion reactor (MFR) applications. They offer good thermal conductivity and lower thermal expansion together with excellent radiation resistance. Figure 1a shows the very low swelling observed in this type of steel relative to either type 316 or advanced Ti-modified austenitic stainless steels after fast breeder reactor (FBR) irradiation to 100 dpa or more [1-5]. However, helium generation during FBR irradiation is very low in martensitic/ferritic steels, as shown in figure 1b, but will be much higher during MFR irradiation to similar displacement-damage doses. Helium is known to affect void swelling in austenitic stainless steels [5,6], and it has been shown to increase void formation in martensitic/ferritic steels as well [7-10]. Helium generation in nickel bearing steels is increased when they are irradiated in the High Flux Isotope Reactor (HFIR), with a mixed fast and thermal neutron spectrum, relative to an FBR like the Fast Flux Test Facility (FFTF), with only fast neutrons. The thermal neutrons produce helium from transmutation reactions with nickel atoms. Martensitic/ferritic steels often contain minor amounts (0.1-0.5 wt %) of nickel to stabilize them against δ-ferrite formation during normalizing treatments. This increases the He/dpa ratio slightly when a steel like 9Cr-1MoVNb (mod. 9Cr-1Mo or T-91) is irradiated in HFIR, as shown in Fig. 1b . If, however, a martensitic/ferritic steel is deliberately alloyed with about 2 wt % Ni, then the ratio of He/dpa generation during irradiation in HFIR increases into the same range expected during irradiation in an MFR first wall, as also shown in Fig. 1b.

For several years, a portion of the MFR materials program at the Oak Ridge National Laboratory (ORNL) has been devoted to studying the sensitivity of

properties and microstructure during irradiation to helium [10-13]. Initial studies have mainly compared the 9Cr-1MoVNb and 12Cr-1MoVW steels irradiated in HFIR with and without Ni-doping, to discern the effects of increased He/dpa ratios. While Ni-doping introduces no obvious microstructural effect on either 9Cr-1MoVNb or 12Cr-1MoVW (HT-9) steels prior to irradiation, other than the need to temper at lower temperatures for longer times (Ni lowers the A_{c1} temperature), it does affect precipitation somewhat during irradiation at 400-500°C, particularly in 9Cr-1MoVNb-2Ni [10,14]. A better comparison would be obtained by irradiating the same material in HFIR and FFTF to obtain different He/dpa ratios at similar temperatures and fluxes. Therefore, the subject of this paper is a comparison of swelling and microstructure of 9Cr and 12Cr steels with and without Ni-doping irradiated in HFIR and FFTF at about 400°C, the temperature of maximum void formation.

EXPERIMENTAL

The compositions of the Ni-doped and undoped heats of 9Cr-1MoVNb and 12Cr-1MoVW are given in Table 1. Standard 3-mm diameter transmission electron microscopy (TEM) disks were punched from 0.25 mm-thick sheet stock, and then these disks were normalized and tempered as indicated in Table 2.

Disks were irradiated in experiment CTR-30 in HFIR at 400°C to neutron fluences producing 36 - 37 displacements per atom (dpa) and 30 - 430 at. ppm He, depending on the Ni content of the alloy. Irradiation conditions and damage parameters for various steels are found in Table 3. Disks were also irradiated in basket 1E2 for cycles 4-6 in the Materials Open Test Assembly (MOTA) of FFTF at 407°C to neutron fluences producing 47 dpa and about 5 at. ppm He in all the alloys. Temperatures in FFTF are recorded during irradiation whereas temperatures

in HFIR are determined by heat transfer calculations that have been verified by post-irradiation examination of monitors that measure temperature during irradiation [15]. Temperature uncertainties for experiments in both reactors appear to be ± 15-25°C or less. Displacement damage is calculated in both reactors from dosimetry measurements. For the HFIR experiment, both dpa and He levels were calculated by L.R. Greenwood [16], and dpa values include the extra contribution of nickel recoils when helium atoms are generated.

TEM specimens were thinned using an automatic TENUPOL electropolishing unit (with cooling) located in a hot cell. TEM disks were examined using a JEM 100C electron microscope equipped with a special objective lens polepiece that lowers the magnetic field at the ferro-magnetic specimen. Quantitative cavity statistics and swelling values were obtained using a ZEISS particle analyzer; foil thicknesses were measured via stereomicroscopy. Some selected area electron diffraction (SAD) was performed in-foil to obtain crystallographic data for phase identification but good, low-order zone axis patterns (ZAPs) were difficult to obtain because tilting more than 5-10° is difficult with magnetic specimens.

Precipitates were also extracted onto carbon replica films from as-tempered and from irradiated samples for phase identification and compositional evaluation using X-ray energy dispersive spectroscopy (XEDS) and convergent beam electron diffraction (CBED). Replicas from the irradiated specimens were prepared in a special shielded hands-on facility because the HFIR specimens in particular were highly radioactive. XEDS was performed on either a Philips EM400T/FEG or a JEM 2000FX (LaB_6) analytical electron microscope (AEM). The EM400T/FEG has a field emission gun (FEG) that produces a very high electron intensity at probe sizes as small as 3nm in diam., so that the compositions of very small precipitate particles could be measured easily. XEDS spectra were quantified after measuring integral

peak intensities using well- established standardless analysis techniques [17,18]. Individual elemental XEDS peaks contained 100-100,000 counts, giving a statistical significance of ± 10-0.3% of the reported composition in atomic percent. Multiple particle measurements were made for each phase identified on the replica.

RESULTS

Cavity Evolution and Swelling - FFTF Irradiation

There were very few voids (large cavities, bias-driven growth), no detectable bubbles (very small cavities, gas-driven growth) and, therefore, negligable cavity swelling in any of the 9Cr and 12Cr steels irradiated in FFTF to 47 dpa at 407°C. Cavity behavior and statistics are described in Table 4, and TEM microstructures of 9Cr and 12Cr steels with and without Ni-doping are shown in Fig. 2. Some large matrix voids (7-23nm in diam.) can be seen in the 9Cr-1MoVNb steel (fig. 2a), and some are occasionally observed within χ phase particles in the 9Cr-1MoVNb-2Ni steel. Large voids (15-23 nm in diam.) are found only occasionally in the 12Cr-1MoVW or 12Cr-1MoVW-2Ni steels.

Cavity Evolution and Swelling - HFIR Irradiation

Abundant void (7-30 nm in diam.) formation was found in both the 9Cr-1MoVNb and 12Cr-1MoVW steels and those doped with 2 wt.% Ni after HFIR irradiation at 400°C to 36-37 dpa, as shown in Fig. 3. Previous work on HFIR irradiation of these steels at 300-600°C established that void formation was maximum at about 400°C [10]. Very few fine helium bubbles (2-5 nm in diam) were

detected in the undoped 9Cr and 12Cr steels despite increased void formation relative to FFTF, as shown for 9Cr-1MoVNb at higher magnification in Fig. 4. Since the TEM resolution limit for bubbles is about 1.5 nm, these steels could contain subcritical bubbles. By contrast, the Ni-doped steels with much more helium, also had much higher concentrations of fine bubbles than found in FFTF, as shown for 9Cr-1MoVNb-2Ni in Fig. 5. Cavity behavior is described and quantitative microstructural data are presented in Table 4.

Swelling due to cavities was 0.3-0.35% in the 9Cr-1MoVNb and 9Cr-1MoVNb-2Ni steels, and slightly less, 0.23-0.25%, in the 12Cr-1MoVW and 12Cr-1MoVW-2Ni steels. While these are not alarmingly high levels of swelling, closer inspection of microstructural details suggests additional insight into the actual stage of void evolution that each specimen is experiencing, which in turn is important to any projections of behavior at higher doses. The swelling in the 9Cr-1MoVNb and 12Cr-1MoVW steels is primarily due to voids. Cavity size distributions plotted from the larger cavities observed in the microstructures show broad tails at larger sizes in these undoped steels (Fig. 6). Calculations accounting for the helium needed to fill these cavities *(cavity character ratio* - generated appm He/calculated appm He for equilibrium bubbles) indicate that these cavities are quite empty, suggesting that they are voids; any accomodation of helium in unresolved bubbles would further support this assessment. Swelling in the 9Cr-1MoVNb-2Ni and 12Cr-1MoVW-2Ni steels is due to the abundant populations of both fine helium bubbles voids. Bubbles cause about 50-66% of the measured swelling in the Ni-doped steels. While the generated helium can be accomodated in the visible cavity microstructure, all the helium could easily fit into the smallest cavities as equilibrium helium bubbles, again suggesting that the larger cavities are probably voids.

The Ni-doped 9Cr and 12Cr steels with 400-430 appm He both have high concentrations of fine bubbles (2-5 nm diam., 1.6-3.5 x 10^{22} m^{-3}) with much lower concentrations (6 and 22 times less, respectively) of larger voids (see Table 4). Void formation in the presence of these dense populations of fine bubbles appears to be similar or somewhat retarded in the Ni-doped relative to the undoped steels. Cavity size distributions in both Ni-doped steels (Figs. 6b and 6d) show shifts in the size distributions toward smaller sizes. The 9Cr-1MoVNb-2Ni steel in particular has fewer voids in the 17-35 nm diameter size range than does the 9Cr-1MoVNb steel. The void densities (neglecting the patchy, spacial nonuniformity in the undoped steel) are similar in the 9Cr steels with and without Ni, but there are noticably fewer voids in the 12Cr steel with Ni as compared to the one without. It would appear, therefore, that the increased density of bubble-sinks was affecting void formation and growth in the Ni-doped steels with the highest helium contents.

Cavity size distributions determined from higher magnification pictures that include both fine bubbles and large voids from the 9Cr-1MoVNb-2Ni and 12Cr-1MoVW-2Ni steels are shown in Fig. 7. These distributions with their large peaks at small sizes and broad tails to larger sizes empirically suggest that the critical cavity size is about 5 nm in diameter in the 9Cr-1MoVNb-2Ni steel, and is about 5-6 nm in diameter in the 12Cr-1MoVW-2Ni steel. Cavities below this size would be stable, sub-critical bubbles, while the larger cavities would have converted from bubbles to unstable, rapidly-growing voids. By contrast to the steels with more helium, critical cavity sizes in the undoped steels irradiated in HFIR or any of the steels irradiated in FFTF appear to be below the TEM resolution limit, or less than 1.5 nm in diameter.

To summarize, the effects of increased helium generation on void and bubble formation can best be seen by comparing FFTF and HFIR irradiation for each heat

of steel. In the 9Cr and 12Cr steels without Ni-doping, a modest increase in helium generation causes a considerable increase in void formation. In the 9Cr and 12Cr steels with Ni-doping, a large increase in helium generation not only increases void formation in HFIR relative to FFTF, but also greatly increases fine bubble nucleation. Both groups of samples appear to be still in the early stages of void formation. The critical cavity size appears to be below the resolution limit of the microscope in all of the FFTF-irradiated steels as well as in the HFIR-irradiated steels without Ni. If this critical size does not change, then it is easy for more voids to form as more helium is generated. In the Ni-doped steels irradiated in HFIR, however, the critical cavity size becomes much larger while void formation becomes somewhat more difficult. These observations consistently suggest that the higher total density of helium bubbles are becoming dominant sinks to hinder void formation.

Dislocation and Subgrain Boundary Structure Evolution - FFTF and HFIR Irradiation

By contrast to the large differences in cavity behavior between steels irradiated in FFTF and HFIR, there is little or no difference in the dislocation or subgrain boundary structure evolution of a given steel irradiated in FFTF and HFIR. There are, however, differences in the evolution of this portion of the microstructure among the various heats of steel that depend on alloy composition and/or tempering conditions.

All of the irradiated steels had moderately to densely tangled dislocation networks that were spacially quite uniform, with a few larger loops visible. The 9Cr-1MoVNb steel irradiated in HFIR at 400°C had a total dislocation density (Λ) of 6×10^{13} m^{-2}, while the 9Cr-1MoVNb-2Ni had a higher Λ of 4×10^{14} m^{-2}. The disloc-

ation structure in the as-tempered material was, by comparison, spacially quite non-uniform from grain to grain, with the degree of non-uniformity depending on the tempering conditions. The 9Cr-1MoVNb steel tempered for 1h at 760°C was most non-uniform. This steel had a network dislocation density (Λ) that varied from 1-7×10^{13} m^{-2} within larger subgrains of the tempered martensite lath structure. The dislocation density was much less in many of the smaller subgrains, but Λ was quite high within the planar honeycomb arrays of dislocation network that defined most of the subgrain boundaries. Subgrains were somewhat smaller, but still had similar or higher dislocation concentrations in 9Cr-1MoVNb-2Ni tempered for 5h at 700°C [18]. In both 9Cr steels, irradiation obviously altered the dislocation structure, as can be seen in Fig. 8 for 9Cr-1MoVNb-2Ni irradiated in FFTF. This involves both some recovery of the as-tempered structure as well as the formation of new dislocations during irradiation. Although a detailed Burger's vector analysis was not done in this work, others have shown that unirradiated ferritic material has network segments of $a_o/2$ <111>, while such material irradiated at 400-500°C develops a structure with a mixture of $a_o/2$ <111> and a_o <100> Burger's vectors [3,19]. Dislocation concentrations in the 9Cr steels are either similar or slightly higher after irradiation at 400°C, but they are also spacially much more uniform compared to unirradiated material. This is most likely related to the significant coarsening of the as-tempered lath subgrain boundary structure that also occured in the 9Cr steels irradiated at 400°C (Figs 8 and 9).

The as-tempered grain and subgrain structure in various steels consists of large prior austenite grain boundaries and packet boundaries around groups of similarly aligned martensite laths, with both boundaries containing coarse $M_{23}C_6$ precipitates along them, and low-angle lath subgrain boundaries, which occasionally have coarse $M_{23}C_6$ or MC particles at junction points. The lath subgrain boun-

daries within the packet boundaries are almost completely removed during irradiation of the 9Cr steels irradiated in either HFIR or FFTF at about 400°C, as seen for 9Cr-1MoVNb-2Ni in Figs. 8 and 9. This can easily be seen in TEM because large regions of irradiated material have uniform contrast, whereas the as-tempered steel has a speckled appearance because contrast conditions change with the slight angular misorientations from lath to lath (Fig. 8 and 9).

In comparison to the behavior of the irradiated 9Cr steels, the as-tempered lath subgrain boundary structure in both of the 12Cr steels remains quite stable during irradiation in either FFTF or HFIR at 400°C. Within the larger subgrains of 12Cr-1MoVW tempered for 2.5h at 780°C, Λ is very low, less than 1×10^{12} m^{-2}. After irradiation in HFIR at 400°C, Λ is 3.5×10^{14} m^{-2}, so that the dislocation concentration in this steel has increased considerably during irradiation, as shown in Fig. 10. The 12Cr-1MoVW-2Ni steel tempered for 5h at 700°C had a finer subgrain size and higher dislocation content within the subgrains prior to irradiation, so that irradiation produced only a modest increase, if any, in the dislocation content of this material.

In summary, irradiation at about 400°C clearly increases the dislocation concentration in the 12Cr-1MoVW steel that had a low dislocation content beforehand by virtue of its tempering conditions (higher temperature, longer time). Irradiation did not produce large increases in dislocation content of the other steels (12Cr-1MoVW-2Ni, 9Cr-1MoVNb, 9Cr-1MoVNb-2Ni), which had higher as-tempered dislocation contents to begin with. Irradiation did, however, evolve a more uniform dislocation network structure that includes some loops and probably a mixture of Burger's vectors. Irradiation appeared to cause almost complete recovery of the as-tempered lath subgrain boundary structure in both the 9Cr steels, while such subgrain boundaries remained stable in the 12Cr steels during irradiation. All

aspects of dislocation/subgrain boundary evolution were identical when comparing the same steels irradiated in HFIR and FFTF.

Phase Formation and Stability - As-Tempered Precipitation

Tempering for the range of conditions shown in Table 2 produced carbide precipitation that differed between 9Cr and 12Cr steels, but was not affected by Ni doping. Table 5 lists phases and their relative abundances, while Tables 6 and 7 give the compositions of the $M_{23}C_6$ and MC phases, respectively, as determined by XEDS analysis on carbon film extraction replicas.

The 9Cr-1MoVNb and 9Cr-1MoVNb-2Ni steels have abundant coarse $M_{23}C_6$ and some finer MC distributed along the prior austenite grain boundaries, along some of the lath subgrain boundaries, and at junction points. The $M_{23}C_6$ phase contains primarily Cr with some Fe and lesser amounts of Mo and V (Table 6). Most of the finer MC phase particles are mainly rich in V (>60 wt.%) with some Cr and Nb. A few MC particles have more Nb (>50%) than V (26-33%) with some Cr (Table 7). Bulk extraction techniques measured 1.4 wt.% of total carbide precipitates in the 9Cr-1MoVNb [7,8], and broad-beam AEM analysis of relative phase fractions on extraction replicas indicates that 85% of the precipitate is $M_{23}C_6$ and 15% is MC. Precipitate phases, fractions and compositions were about the same in 9Cr-1MoVNb and 9Cr-1MoVNb-2Ni steels.

The 12Cr-1MoVW steel contains more carbide precipitation (3.5 wt.%) after tempering than the 9Cr steels, with relative amounts of 99% $M_{23}C_6$ and 1% MC. All the MC is V-rich because these steels contain no Nb. Although a lower tempering temperature refines the $M_{23}C_6$ size distribution somewhat in the 12Cr-1MoVW-2Ni, there is otherwise no obvious effect of Ni doping on the precipitation.

Phase Formation and Stability - Evolution of $M_{23}C_6$ During FFTF and HFIR Irradiation

The as-tempered, coarse $M_{23}C_6$ precipitation appears to become unstable during irradiation of 9Cr-1MoVNb and 9Cr-1MoVNb-2Ni at 400-410°C in FFTF and HFIR, dissolving at lath subgrain boundaries and somewhat along packet boundaries. This phase instability is coincident with the coarsening of the subgrain boundary structure noted above. While no additional precipitation occurs in the 9Cr-1MoVNb steel during irradiation (Figs. 2a, 3a and 4), abundant formation of new, coarse $M_{23}C_6$ particles occurs uniformly within the large matrix regions of the 9Cr-1MoVNb-2Ni steel that are free of prior martensite lath subgrain boundaries (Figs. 2b, 3b, 5, 8, and 9). Figure 9 of 9Cr-1MoVNb-2Ni irradiated in FFTF, shows coarse $M_{23}C_6$ particles at prior austenite grain boundaries and lath packet boundaries with odd, elongated shapes. These irregular shapes suggest that discrete smaller particles have grown together to form the larger ones. The composition of these irradiation-produced $M_{23}C_6$ particles is slightly different from the as-tempered phase (Table 6), with somewhat more Ni and Si, and slightly less Cr, Fe and V, but still well within the characteristic compositional range for that phase [6]. While this abundant precipitation of $M_{23}C_6$ is a noticable difference between the behavior of the Ni-doped and the undoped 9Cr steels during irradiation (Figs. 2a and 2b, and 3a and 3b), it is important to note that the production, distribution and composition of these particles in the 9Cr-1MoVNb-2Ni steel is about the same in FFTF and HFIR (Fig. 2b and 3b). There is some replacement of coarse $M_{23}C_6$ along boundaries by similarly coarse M_6C in the 9Cr-1MoVNb-2Ni irradiated to 47 dpa in FFTF (Table 5).

The as-tempered $M_{23}C_6$ is quite stable during irradiation of the 12Cr-1MoVW and 12Cr-1MoVW-2Ni steels in either FFTF or HFIR, in contrast to the instability found in the 9Cr steels. Irradiation does not produce additional $M_{23}C_6$ nor does it alter its composition. The Ni-doped 12Cr steel experiences some replacement of coarse $M_{23}C_6$ along boundaries by coarse M_6C during irradiation, similar to observations made in 9Cr-1MoVNb-2Ni, but this behavior is the same during both FFTF and HFIR irradiation (Table 5).

Phase Formation and Stability - Evolution of MC During FFTF and HFIR Irradiation

The as-tempered, finer MC precipitation also appeared to be unstable during irradiation in all the steels. The MC coarsened and became more abundant, especially in the 9Cr steels, as illustrated in Fig. 11 for 9Cr-1MoVNb irradiated in HFIR. Coincident with the microstructural coarsening, there was a considerable change in the composition of the MC phase during irradiation, as shown in Table 7 and in Fig. 12. The V-rich MC particles with low Nb contents were more abundant, and could be easily distinguished from the sparce Nb-rich MC particles in the irradiated 9Cr steels. The two types of MC were similarly distinct in the as-tempered, unirradiated material. Both types of MC carbides became much richer in Cr at the expense of V (Fig. 12). Trace levels of Si, Ni, Fe and Mo were also detected in the irradiation-produced MC particles, but these were minor changes relative to the changes in Cr and V concentrations. There were some small differences in the effects of irradiation on the MC phase composition between the Ni-doped and undoped 9Cr steels in HFIR, but almost no differences between these steels after FFTF irradiation (Table 7). Most importantly, there was little or no

discernable difference in MC phase composition between either 9Cr steel irradiated in HFIR and in FFTF, as emphasized by Fig. 13 for 9Cr-1MoVNb. .

The Cr enrichment and V depletion of MC during irradiation of the 12Cr steels is very similar to that observed in the 9Cr steels. Many MC particles show very high levels of Ti after irradiation in either reactor. The 12Cr steels do not have Nb-rich MC particles before or after irradiation.

Phase Formation and Stability - Evolution of M_6C During FFTF and HFIR Irradiation

Abundant dispersions of fine M_6C (5-40 nm) were produced during irradiation in FFTF and HFIR at 400-410°C in all steels except the 9Cr-1MoVNb steel. These fine particles can be easily seen at higher magnification in Fig. 14. Diffraction information is consistent with the very similar crystal structures of either $M_{23}C_6$ (face-centered cubic) or M_6C (diamond cubic), but the Si, Cr and Ni-rich phase composition found clearly indicates that this phase is M_6C (η) (Table 8). The phase composition is about the same as the Si-Cr-Fe-Ni-Mo composition found for M_6C (η) in type 316 stainless steel irradiated in HFIR at 425-450°C, where the diamond cubic crystal structure has been positively identified by careful electron diffraction [20].

Similarly fine particles were found in the microstructure of the 12Cr-1MoVW steel after irradiation at about 400°C. These particles have an odd composition that is very rich in Si and Cr, has minor levels of Fe, Mo and/or Nb, V, but has little or no Ni. The in-foil diffraction characteristics (where tilting is limited) are the same as found for the Ni-rich M_6C (η) in the other steels. Gelles and Thomas [3] have observed abundant, fine Cr-rich α' precipitation in similar steels, but our compositional and diffraction results do not suggest α'. More work needs to be

done to positively identify this phase; it is, however, consistently found in both HFIR- and FFTF-irradiated specimens.

As mentioned in the above section on the evolution of $M_{23}C_6$, irradiation at 400°C produces some coarse M_6C that replaces coarse, as-tempered $M_{23}C_6$ particles along prior austenite grain and lath-packet subgrain boundaries, but only in the Ni-doped steels (Table 5). Replacement is not noticable in the in-foil microstructure, but becomes quite obvious during XEDS analysis on extraction replica films. Such coarse M_6C forms to a limited extent in 9Cr-1MoVNb-2Ni, but only during FFTF irradiation. More replacement M_6C particles form in 12Cr-1MoVW-2Ni in both reactors relative to 9Cr-1MoVNb-2Ni, but they occur more frequently during HFIR irradiation.

Despite some differences in formation characteristics and phase composition between finer and coarser M_6C particles in the various heats of steel, fine M_6C (η) precipitation is exactly the same in the various steels after FFTF and after HFIR irradiation. The fine M_6C phase composition is the same in both reactors, as emphasized in Fig. 15 for 9Cr-1MoVNb-2Ni. Even the composition of the fine, Ni-poor particles found in the 12Cr-1MoVW steel is fairly similar after HFIR and after FFTF irradiation (Table 8).

Phase Formation and Stability - Evolution of Other Phases

Traces of the fine, acicular M_2X needles, rich in Cr (75 at.%) and V (~20%) were found only in 9Cr-1MoVNb irradiated in FFTF. Some coarser particles with the same composition were found along boundaries in the 9Cr-1MoVNb-2Ni steel irradiated in FFTF. Although abundant formation of fine G phase ($Mn_6Ni_{16}Si_7$) particles has been observed by others in similarly irradiated steels [3, 4, 21], we

found no G phase in any of our steels irradiated in FFTF and HFIR at 400-410°C. We have, however, previously reported detecting trace levels of fine G phase precipitation in the 12Cr-1MoVW steel irradiated in HFIR at 500°C [10].

DISCUSSION

The first portion of the discussion will compare the present swelling and microstructural data with data of others on similar steels, mainly from neutron experiments. The remainder will focus on the clear role that increased helium generation plays to enhance void formation in these martensitic/ferritic steels, and the implications of such effects on the mechanism affecting or controlling void formation. Results on the evolution of other microstructural components will be discussed in the context of their relationship to the cavity microstructure. In general, except for cavities, microstructural evolution was similar for FFTF and HFIR irradiations of the same steel and, therefore, relatively unaffected by changes in helium level. Thus, these experiments can be interpreted as effectively straightforward, single-variable experiments of helium effects on cavity evolution, even in the steels doped with Ni.

The FFTF void-swelling behavior of the 9Cr and 12Cr steels (T91 and HT-9 base compositions, respectively) used in this work are generally consistent with the growing body of high-fluence FBR data on the martensitic class of ferritic steels [22-25]. This class includes such other steels as EM-12 (9Cr-2MoVNb, France), FV448 (12Cr-0.5MoVNb, United Kingdom), and DIN 1.4914 (12Cr-0.5MoVNb, West Germany). These steels have very good void-swelling resistance, with <0.6% swelling at doses of 100-125 dpa. Some coarse voids were seen in EM-12 at ~100 dpa by

Gelles after EBR-II irradiation [23]. Our FFTF results, which show a few voids in the 9Cr steel and almost none in the 12Cr steel, are consistent with these observations.

There have been previous microstructural observations made on duplicate 9Cr-1MoVNb and 12Cr-1MoVW specimens irradiated in HFIR at 400°C to ~37 dpa by Vitek and Klueh [7,8], and by Gelles and Thomas [3,14] on a similar heat of 12 Cr-1MoVW (but with a different heat treatment) irradiated in HFIR at 400°C to 10 and 39 dpa. Gelles and Thomas also compared EBR-II irradiated HT-9 with their HFIR results to analyze for possible helium effects. For the 9Cr-1MoVNb steel, we found more of the smaller cavites and slightly more swelling than Vitek and Klueh [8], but otherwise the cavity results are similar. For the 12Cr-1MoVW steels, we measured several times more swelling and almost 10 times more cavities (mainly smaller ones) than Vitek and Klueh [9], but such differences are not unexpected, given the microstructural heterogeneity of these steels. Gelles and Thomas [3] found no effect of helium after 10 dpa in HFIR relative to EBR-II irradiation. On the other hand, Gelles [9] found that cavity formation is enhanced after 39 dpa in HFIR, but observed fewer and smaller cavities than we did, and about 4 times less swelling. Our reactor data on the Ni-doped steels are unique.

There have also been dual-ion irradiation experiments on these or similar steels to investigate helium effects on cavity formation [26-29]. Work by Ayrault [26], using the dual-ion beam facility at the Argonne National Laboratory (ANL), showed that helium was essential to void formation at 410-470°C after 25 dpa in the same heats of 12Cr-1MoVW and 12Cr-1MoVW-2Ni used in the present work. The Ni-doping actually suppressed void swelling at 470°C. Farrell and Lee [27,28], using the dual ion facility at ORNL, found that bias-driven voids could form at 450-550°C in 9Cr-1MoVNb (the same heat as used in this work) and 10Cr-6MoNb steels after

100 dpa. They found that helium enhanced void formation to produce maximum swellings of 0.4% and 0.75%, respectively, in the two steels. Horton and Bentley [29], also using the ORNL facility, found that dual- and triple (deuterium + tritium)-ion beam irradiations of a binary Fe-10Cr alloy at 580°C produced a significant enhancement in void swelling after irradiation to 100 dpa (1.2 and 2.5% swelling, respectively).

There are few data available on the dislocation density in neutron irradiated 9Cr-1MoVNb or 12Cr-1MoVW steels. Our 400°C values of Λ for 9Cr-1MoVNb are considerably less than the values measured after ion irradiation at 400-500°C by Farrell and Lee [27]. The range of Λ observed in our various steels irradiated in different reactors at 400-410°C ($0.6\text{-}3.5\times10^{14}$ m^{-2}) is also significantly less than the values observed by Gelles [30] for binary Fe-9Cr and -12Cr alloys irradiated in EBR-II at 400-450°C, or those observed by Horton and Bentley in ion-irradiated Fe-10Cr at ~580°C. Besides our data, there appear to be no other observations on subgrain structural instability during irradiation [10].

Comparison of our precipitation results with the results of others and discussion about the role of radiation-induced solute segregation has been made elsewhere [10,21]. Our observations of fine M_6C (η) in irradiated HT-9 are consistent with findings by Little and Stoter [31] on FV 448. Our results differ considerably from those of Gelles and co-workers [3,9], who report abundant precipitation of fine G and α' phases in 12Cr-1MoVW irradiated in EBR-II and HFIR at 400-500°C. Our obsevations of radiation-produced $M_{23}C_6$ in the Ni-doped 9Cr steel and compositional modification of the MC phase in the various steels appear to be new findings.

There has been a considerable amount of theoretical work directed towards understanding the mechanisms that control void formation and swelling in ferritic steels, particularly during FBR irradiation, where the resistance to void swelling is

so obvious relative to austenitic stainless steels. Two recent reviews highlight the important mechanisms to consider [25,32]:

a.) *Low intrinsic bias* - This effect includes factors suggested to be inherent to the BCC crystal structure of the material. Sniegowski and Wolfer [33] proposed that the preferential attraction of dislocations for interstitials relative to vacancies (bias) is lower in BCC than in FCC materials because self-interstials have smaller relaxation volumes in BCC material. Odette [32] also pointed out that self-diffusion rates are considerably higher in BCC relative to FCC iron, which would enhance defect recombination.

b.) *Low bias due to dislocation nature* - Bullough and co-workers [34,35] proposed that a_o<100> loops with a strong interstitial bias cause the more neutral $a_o/2$<111> dislocation sinks to absorb vacancies, thus competing with cavities to reduce the net bias of the system.

c.) *Solute effects* - Little [36,37] and others [38] have suggested that there is substitutional trapping of point defects by solute atoms in BCC steels. Little [36] also suggested that substitutional solutes segregating to dislocations can reduce their bias for interstitials and inhibit climb. Both effects enhance point defect recombination. Gelles [39] has recently observed reduced swelling with oversize misfit solute atoms in dilute binary alloys and suggested radiation-induced segregation to dislocations and void surfaces was responsible.

d.) *Microstructural sink balance effects* - Horton and Mansur [40], in the context of a rate theory study of cavity growth rates and critical cavity size, indicated that domination of the microstructure by either dislocation or cavity sinks also contributes to the low swelling observed in BCC materials. Imbalanced partitioning leads to enhanced point defect recombination at the dominant sink. Their Fe-10Cr results suggest cavity-dominated microstructures, whereas similar interpretation of results on 9-10Cr steels indicated dislocation-dominated microstructures at low gas levels, and cavity dominated structures at high gas levels.

e.) *Microstructural lath/subgrain boundary effects* - Ayrault [26] and Maziasz et al. [10] have suggested that these boundaries are strong neutral sinks which enhance point defect recombination and lower the vacancy supersaturation in the as-tempered commercial steels.

f.) *Microstructural precipitation effects* - Gelles and Thomas [3] suggested that the fine G and α' precipitates that have been observed under irradiation contribute to void swelling resistance.

g.) *Gas effects* - Ferritic steels without Ni have lower helium generation rates during FBR irradiation than austenitic steels because Ni has a much higher (n,α) cross-section than Fe or Cr. All of the studies on the effect of helium [7-10, 19, 26-29] point to its stimulation of void nucleation. Triple-ion beam experiments also show an enhanced effect of helium and hydrogen together [19, 27-29].

Most of these mechanisms relate to the vacancy supersaturation availible for void nucleation and growth. However, gas effects (g) and the critical size, r_c, for conversion of a stable gas bubble into a bias-driven void [32, 40 and 41] are most relevant to void nucleation, which is the major issue addressed by our data. While most of the above-mentioned mechanisms probably contribute in concert to the void-swelling resistance observed in these steels during FBR irradiation, our data suggest that mechanisms d.) and e.) are most important to void growth during irradiation at higher helium generation levels.

Our data indicates that void nucleation is very difficult during FBR irradiation with little or no helium, and that increased helium generation greatly enhances void nucleation. Void nucleation can occur in austenitic stainless steels even without any helium present due to oxygen effects [42,43], and elemental Ni used for alloying can have very high oxygen contents, usually higher than the Cr or Fe starting stock used to produce austenitic alloys and steels [44]. The martenistic/ferritic steels contain little Ni and much higher C contents (C is a very efficient deoxidizing element, as are Si and Ti) compared to austenitic steels and alloys, so that they most likely have less oxygen available for void nucleation and are more dependent on helium generated during irradiation.

Macroscopic swelling with increasing fluence can be described in terms of a low-swelling transient regime or incubation period, followed by a steady-state regime of much more rapid swelling [6,20]. Voids nucleate and grow during the low-swelling transient regime, and usually rapid void growth and/or coalescence cause the onset of rapid swelling. Our data suggest that, while helium appears to have accelerated void nucleation to shorten the incubation period, perhaps by 75-100 dpa or more, none of our microstructures appear to be at the end of the transient regime and certainly not into the rapid-swelling regime.

Two closely related critical parameters from rate theory, the critical radius, r_c, and the critical number of gas atoms, n_g^*, whose mathematical equations are described by Odette [32] and Mansur and Coghlan [41], help to interpret our microstructural data. Our data suggest empirical estimates for r_c; n_g^* is more difficult to estimate, but can be related to the duration of the incubation period. The r_c for the undoped 9Cr and 12Cr steels in this work appears to be <0.75 nm at 400-410°C in both FFTF and HFIR, whereas in the Ni-doped steels r_c increases from that value in FFTF to 2.5-3 nm in HFIR. The void formation in 9Cr-1MoVNb in FFTF may also indicate a very low value of n_g^* in that steel. At low values of both r_c and n_g^*, more helium would readily lead to more voids, as we observe for the undoped 9Cr and 12Cr steels irradiated in HFIR. Void formation appears more difficult in the Ni-doped steels in HFIR because r_c and, presumably n_g^*, increase. But void nucleation still increases. The value of r_c for the undoped steels appears to be consistent with that expected by others at about 400°C based on ion irradiation data [27, 28, 40], but the value of 2.5-3 nm in the Ni-doped, HFIR irradiated steels seems large, as large as Horton and Mansur [40] find for Fe-10Cr ion irradiated at 580°C to 30 dpa. In SA 316 irradiated at 425-450°C, voids form easily and r_c appears to be ~1.5 nm, while in CW 316 or Ti-modified austenitic stainless steels that are resistant to void formation in HFIR at 400°C, r_c > 2.5-5 nm [20, 45].

Void formation and growth are also affected by the net bias or vacancy supersaturation and defect partitioning. The HFIR results on the Ni-doped steels with large r_c may suggest a larger vacancy supersaturation than might be anticipated and a more balanced partitioning of point defects among various sinks, despite the high density of bubbles. We can calculate a point defect partitioning factor Q for either vacancies or intersitials, defined for a two sink system as [41]

$$Q = Z^d \Lambda / 4\pi r N_c Z^c \qquad (1)$$

where , Z^d and Z^c are the capture efficiencies of dislocations and cavities, respectively for that particular defect (usually ~1), Λ is the dislocation density, r is the average cavity radius, and N_c is the cavity concentration. Horton and Mansur [40] give an expression for the sink strength that includes a bimodal cavity distribution. The sink strength, S, for vacancies or interstitials can be expressed generally to include other sinks as follows,

$$S = 4\ \Sigma_i r_i N_{c,i} Z^c(r_i) + \Lambda Z^d + \Gamma Z^b + 4\ \Sigma_j r_{p,j} N_{p,j} Z_p(r_{p,j}) \qquad (2)$$

where the first term sums over a cavity distribution with *i* size classes, Γ is concentration of subgrain boundaries, *j* is the number of precipitate types with average size r_p and concentration N_p, and Z^b and Z^p are the capture efficiencies of subgrain boundaries and precipitates, respectively, for vacancies or interstitials. Using the simple form of eq. 1, our steels irradiated in FFTF have Q>40 so that they appear to be dislocation sink dominated. The values of Z^d and Z^c are assumed to be = 1 and values for the other parameters in eq. 1 are obtained from the experimental data. The undoped steels irradiated in HFIR have Q~0.2, while the Ni-doped steels have Q~0.4, including the contribution of the bimodal cavity distribution. Clearly the HFIR irradiated specimens are closer to a balanced situation than the FFTF irradiated steels, and yet do not appear to have a sink structure totally dominated by cavities as do many cold-worked austenitic stainless steels irradiated in HFIR. The calculated Q values for the HFIR irradiated steels could be either closer or further from a balanced sink situation, depending on how the precipitates

and subgrain boundaries compete with other sinks for point defects. The finer subgrain boundary structure may be a factor in reducing void formation and growth in the 12Cr-1MoVW-2Ni irradiated in HFIR.

Considering the bias, theoretical work suggests that the bias (B) in the ferritic steels can range from 0.05 to 0.4 [40]. The normal B for austenitic steels is 0.15-0.2 [32]. We cannot really estimate bias simply from void formation without knowing growth rates. However, it seems that enough bias exists for substantial void growth in these ferritic steels. From the various mechanisms that contribute to a low bias in ferritic steels, solute effects and dislocation nature effects appear constant in our comparison of FFTF and HFIR irradiation for each steel, and appear small among the various steels in either reactor. Helium generation itself could counter the low intrinsic bias suggested in mechanism a.) if helium trapped in vacancies hinders recombination with interstitials as suggested for austenitic steels [6,20]. Helium vacancy complexes may also be more mobile in the ferritc steels if the vacancy self-diffusion rate is higher. Increased helium accumulation at various sinks, governed by D_vC_v (vacancy diffusivity × vacancy concentration) in the ferritic steels, could also alter defect capture efficiencies. Apart from defect-partitioning effects, subgrain boundaries and precipitates could also affect the bias as well. Fine precipitates could contribute to an increase in the bias if they preferentially attract interstitials on the basis of their volumetric misfit (undersized misfit would attract interstitials). Fine precipitates do not appear to contribute very much to void swelling resistance from this work, because void formation in HFIR often coincides with their formation. Previous data at 500°C actually show that fine M_6C develops cooperatively with voids in HFIR-irradiated 12Cr-1MoVW [10].

Finally, what do these results mean for the use of ferritic steels for fusion applications? While swelling in these 9Cr and 12Cr steels is not high and may not increase greatly at higher doses, several factors could still contribute to higher eventual void swelling rates during fusion irradiation than found during FBR irradiation. The voids in the steels with the fusion levels of helium could continue to grow, while new voids still form. These processes could then reduce the number of fine bubbles to lower r_c and achieve more balanced defect partitioning, which would further increase swelling. Odette [32] showed that an increase in bias and in the ultimate void density (a normal helium effect in austenitic stainless steels) could result in the ferritic steels swelling in a manner similar to 20% cold-worked type 316 stainless steel. If voids develop on coarse precipitates, swelling could be enhanced still further. Higher fluence experiments are necessary, but until then, the possibility of helium enhanced void swelling remains a legitimate concern for fusion.

SUMMARY AND CONCLUSIONS

1.) By comparing Ni-doped and undoped 9Cr-1MoVNb and 12Cr-1MoVW steels irradiated in FFTF (47 dpa, ~5 appm He) and HFIR (~37 dpa, 400-430 appm He), it was found that increases in He/dpa ratio cause significant increases in the formation of large (7-30 nm diam.), bias-driven voids at 400-410°C. Only the Ni-doped steels irradiated in HFIR with 400 appm He or more had visible helium bubbles, which were very fine (2-5 nm diam) and abundant ($1\text{-}4 \times 10^{22}$ m^{-3}).

2.) Irradiation in both reactors produced a spatially uniform network of tangled dislocations and some larger loops, with Λ being $0.6\text{-}4 \times 10^{14}$ m^{-2}. Irradiation

produced a structure that was different than the initial as-tempered, spatially non-uniform structure in which A varied from $<10^{11}$ to 7×10^{13} m^{-2}. Irradiation significantly increased A only in the 12Cr-1MoVW steel for which had A was initially very low ($<10^{11}$ m^{-2}). Irradiation at 400-410°C produced almost complete recovery of the as-tempered lath subgrain boundary structure in the 9Cr-1MoVNb and 9Cr-1MoVNb-2Ni steels. Such boundaries remained stable in similarly irradiated 12Cr-1MoVW and 12Cr-1MoVW-2Ni steels.

3.) Irradiation produced some significant changes in the precipitate structure on all of the steels irradiated at 400-410°C in both reactors. There was dissolution of many of the coarse, as-tempered $M_{23}C_6$ particles during irradiation of both 9 Cr steels, whereas similar particles were relatively more stable in the 12 Cr steels. Irradiation produced an abundant dispersion of new coarse $M_{23}C_6$ particles only in the 9Cr-1MoVNb-2Ni steel. Finer MC precipitate particles, present in all the steels, experienced some coarsening and compositional changes (Cr enrichments and V depletions) during irradiation. Irradiation produced abundant dispersions of fine M_6C (η) in all the steels except 9Cr-1MoVNb. These particles were Si, Cr and Ni rich in the Ni-doped steels, but had an odd composition with only Si and Cr in the 12Cr-1MoVW steel. Some coarse M_6C (η) (Si, Cr and Ni rich) was found to replace coarse as-tempered $M_{23}C_6$ during irradiation in both Ni-doped 9 Cr and 12 Cr steels.

4.) Although irradiation at 400-410°C had considerable effects on both the dislocation and subgrain boundary and the precipitate components of the microstructure in all the steels, these changes were nearly the same comparing irradiation in FFTF and HFIR for each heat of steel.

5.) Interpretation of our data within the framework of existing rate theory and modeling indicates that there is a sufficient bias for void growth in ferritic/martensitic steels irradiated at about 400°C if there is enough helium for voids to nucleate. Our data indicates that the critical size and critical gas content for the conversion of stable gas clusters or bubbles (r_c and n_g^*, respectively) to voids are quite small (r_c<0.75 nm) in the 9Cr-1MoVNb and 12Cr-1MoVW steels irradiated in both reactors, because more helium causes more voids without producing resolvable bubbles. The higher helium content of the Ni-doped steels irradiated in HFIR produces many resolvable, but sub-critical, helium bubbles, which increases r_c to 2.5-3 nm; however, voids still form and grow indicating the presence of some bias. All of the steels irradiated in FFTF appear to have point defect annihilation dominated by the sink strength of the dislocations. By contrast, the increased density of bubbles to act as sinks in the steels irradiated in HFIR appears to cause more balanced defect partitioning. Our data suggest that subgrain boundaries, and possibly precipitate particles, may also be important sinks in the system as well.

6.) Our data clearly shows helium enhanced void formation where the low-swelling transient regime could be shortened by as much as 75-100 dpa. The levels of cavity swelling observed are small, less than 0.5%. However, microstructural details suggest that void formation is in the early stages of development, and that several mechanisms could easily lead to more void nucleation and growth as dose increases. The possibility of helium enhanced void swelling remains a legitimate concern for fusion that higher fluence experiments need to address.

ACKNOWLEDGEMENTS

We would like to thank Dr. J.M. Vitek for earlier work on the Ni-doped steels, particularly preparing specimens for the various reactor experiments. We would also like to thank Noble Rouse for excellent preparation of TEM specimens, especially those that are highly radioactive after HFIR irradiation. We thank Drs. D.A. Pedraza and J.M. Vitek at ORNL for reviewing this paper.

REFERENCES

1. Huet, J.J., et al., *Proc. Irradiation Behavior of Metallic Materials for Fast Reactor Core Components*, Ajaccio, France (CEA, 1979) p. 5.

2. Erler, J., et al. , *Proc. Irradiation Behavior of Metallic Materials for Fast Reactor Core Components*, Ajaccio, France (CEA, 1979) p. 11.

3. Gelles, D.S. and Thomas, L.E., *Proc. Topcial Conference on Ferritic Alloys for Use in Nuclear Energy Technologies*, eds. J.W. Davis and D.J. Michel (The Metallurgical Society of AIME, 1984) p. 559.

4. Gelles, D.S., *J. Nucl. Mater.* 122-123 (1984) 207.

5. Maziasz, P.J., *J. Nucl. Mater.* 122-123 (1984) 472.

6. Maziasz, P.J. and McHargue, C.J., *Internat. Matls. Rev.*, 32 (1987) 190.

7. Vitek, J.M. and Klueh, R.L., *Proc. Topcial Conference on Ferritic Alloys for Use in Nuclear Energy Technologies*, eds. J.W. Davis and D.J. Michel (The Metallurgical Society of AIME, 1984) p. 551.

8. Vitek, J.M. and Klueh, R.L., *J. Nucl. Mater.* 122-123 (1984) 254.

9. Gelles, D.S., *ADIP Semiannu. Prog. Rept.*, March 31, 1985, DOE/ER-0045/14 (Office of Fusion Energy, U.S. Department of Energy, 1985) p. 129.

10. Maziasz, P.J., Klueh, R.L. and Vitek, J.M., *J. Nucl. Mater.* 141-143 (1986) 929.

11. Klueh, R.L., Vitek, J.M. and Grossbeck, M.L., *J. Nucl. Mater.* 103&104 (1981) 887.

12. Klueh, R.L., Vitek, J.M. and Grossbeck, M.L., *Effects of Radiation on Materials: Eleventh Conference*, ASTM STP-782, eds. H.R. Brager and J.S. Perrin, Am. Soc. for Testing and Matls., Philadelphia (1982) p. 648.

13. Klueh, R.L. and Vitek, J.M., *J. Nucl. Matls.* 117 (1983) 295.

14. Klueh, R.L. and Maziasz, P.J., "Helium Effects on Neutron-Irradiated Cr-Mo Ferritic Steels: A Review of Recent Results," elsewhere in this proceedings.

15. Grossbeck, M.L., Woods, J.W. and Potter, G.A., *ADIP Quart. Prog. Rept.*, Sept. 30, 1980, DOE/ER-0045/4 (Office of Fusion Energy, U.S. Department of Energy, 1981) p. 36.

16. Greenwood, L.R., *ADIP Semiannu. Prog. Rept.*, March 31, 1985, DOE/ER-0045/14 (Office of Fusion Energy, U.S. Department of Energy, 1981) p. 22.

17. Zaluzec, N.J., *Introduction to Analytical Electron Microscopy*, eds. J.J. Hren, J.I. Goldstein, and D.C. Joy, Plenum Press, New York, NY (1979) p. 121.

18. Maziasz, P.J. and Klueh, R.L., *ADIP Semiannu. Prog. Rept.*, March 31, 1985, DOE/ER-0045/14 (Office of Fusion Energy, U.S. Department of Energy, 1981) p. 74.

19. Horton, L.L.S., "A Transmission Electron Microscopy Study of Fusion Enviornment Radiation Damage in Iron and Iron-Chromium Alloys," Oak Ridge National Laboratory Report, ORNL/TM-8303 (July 1982).

20. Maziasz, P.J., "Effects of Helium Content on Microstructural Development in Type 316 Stainless Steel During Neutron Irradiation," Oak Ridge National Laboratory Report, ORNL-6121 (November, 1985).

21. Maziasz, P.J., *Materials for Nuclear Reactor Core Applications* (Bristol Meeting, Oct.27-29, 1987), vol.2, British Nucl. Energy Soc., London (1988) p. 61.

22. Harries, D.R., *Proc. Topcial Conference on Ferritic Alloys for Use in Nuclear Energy Technologies*, eds. J.W. Davis and D.J. Michel (The Metallurgical Society of AIME, 1984) p. 141.

23. Gelles, D.S., *J. Nucl. Mater.* 148 (1987) 136.

24. Bagley, K.Q., et al., *Materials for Nuclear Reactor Core Applications* (Bristol Meeting, Oct.27-29, 1987), vol.2, British Nucl. Energy Soc., London (1988) p. 37.

25. Little, E.A., *Materials for Nuclear Reactor Core Applications* (Bristol Meeting, Oct.27-29, 1987), vol.2, British Nucl. Energy Soc., London (1988) p. 47.

26. Ayrault, G., *DAFS Quart. Prog. Rept.*, February, 1982, DOE/ER-0046/8, vol. 1 (Office of Fusion Energy, U.S. Department of Energy), p. 182.

27. Farrell, K. and Lee, E.H., *Effects of Irradiation on Materials: Twelfth International Symposium*, ASTM STP-870, eds. F.A. Garner and J.S. Perrin, Am. Soc. for Testing and Matls., Philadelphia PA (1985) p. 383.

28. Farrell, K. and Lee, E.H., *Radiation-Induced Changes in Microstructure: 13th Symposium (Part I)*, ASTM STP-955, eds. F.A. Garner, N.H. Packan, and A.S. Kumar, Am. Soc. for Testing and Matls., Philadelphia PA (1987) p. 498.

29. Horton, L.L. and Bentley, J., *Proc. Topcial Conference on Ferritic Alloys for Use in Nuclear Energy Technologies*, eds. J.W. Davis and D.J. Michel (The Metallurgical Society of AIME, 1984) p. 569.

30. Gelles, D.S., *J. Nucl. Mater.* 103&104 (1981) 975.

31. Stoter, L.P. and Little, E.A., *Advances in Physical Metallurgy and Applications of Steels*, The Metals Society, London, U.K. (1981) p. 369.

32. Odette, G.R., "On Mechanisms Controlling Swelling in Ferritic and Martenisitic Alloys," to be published in *J. Nucl. Mater.*, 154-156 (1988).

33. Sniegowski, J.J. and Wolfer, W.G., *Proc. Topcial Conference on Ferritic Alloys for Use in Nuclear Energy Technologies*, eds. J.W. Davis and D.J. Michel (The Metallurgical Society of AIME, 1984) p. 579.

34. Bullough, R., Wood, H.M., and Little, E.A., *Effects of Radiation on Materials: Tenth Conference*, ASTM STP-725, eds. D. Kramer, H.R. Brager and J.S. Perrin, Am. Soc. for Testing and Matls., Philadelphia PA (1981) p. 593.

35. Little, E.A., Bullough, R. and Wood, H.M., *Proc. Royal Soc.*, A372 (1980) 565.

36. Little, E.A., *J. Nucl. Mater.*, 87 (1979) 11.

37. Little, E.A. and Stow D., *J. Nucl. Mater.*, 87 (1979) 25.

38. Hayns, M.R. and Williams, T.M., *J. Nucl. Mater.*, 74 (1978) 151.

39. Gelles, D.S., *Fusion Reactor Materials Semiannu. Prog. Rept.*, September 30, 1986, DOE/ER-0313/1, (Office of Fusion Energy, Department of Energy, 1987) p. 150.

40. Horton, L.L. and Mansur, L.K., *Effects of Irradiation on Materials: Twelfth International Symposium*, ASTM STP-870, eds. F.A. Garner and J.S. Perrin, Am. Soc. for Testing and Matls., Philadelphia PA (1985) p. 344.

41. Mansur, L.K. and Coghlan, W.A., *J. Nucl. Mater.*, 119 (1983) 1.

42. Nelson, R.S. and Mazey, D.J., *Radiation Damage in Reactor Materials*, IAEA-SM-120, vol. 2, International Atomic Energy Agency, Vienna, Austria (1969) p. 157

43. Lee, E.H. and Mansur, L.K., "Effect of Residual and Injected Oxygen on Swelling in Irradiated Fe-Ni-Cr Alloys - Part II," submitted to *Phil. Mag.*, 1988.

44. Chemical analyses on steels melted at ORNL, 1986-1988.

45. Maziasz P.J. and Braski, D.N., *J. Nucl. Mater.* 122&123 (1984) 311.

FIGURE CAPTIONS

1. a.) Swelling behavior versus fluence for 20% cold worked (CW) type 316, 20-25% CW advanced Ti-modified austenitic stainless steels and various 9-12 Cr martensitic/ferritic steels irradiated in EBR-II at 450-550°C [1-6]. The trend band for the ferritic steels includes data up to about 100 dpa and is linearly extrapolated to to about 150 dpa. b.) Helium generation versus dose for various ferritic steels irradiated in EBR-II or a fusion reactor first wall, and for 9Cr-1MoVNb with and without 2 wt.% Ni doping irradiated in HFIR.

2. Microstructure of various 9Cr and 12Cr martensitic/ferritic steels irradiated in FFTF at 407°C, to a dose of 47 dpa and helium level of ~5 at. ppm. a.) 9Cr-1MoVNb, b.) 9Cr-1MoVNb-2Ni, c.) 12Cr-1MoVW, and d.) 12Cr-1MoVW-2Ni.

3. Microstructure of various 9Cr and 12Cr martensitic/ferritic steels irradiated in HFIR at 400°C to a dose of ~37 dpa and helium levels that depend on Ni content. a.) 9Cr-1MoVNb (30.5 at. ppm.), b.) 9Cr-1MoVNb-2Ni (402.5 at. ppm.), c.) 12Cr-1MoVW (85.3 at. ppm.), and d.) 12Cr-1MoVW-2Ni (429 at. ppm.).

4. Microstructure at higher magnification in kinematical contrast is used to show fine helium bubbles, when are present, and larger voids in 9Cr-1MoVNb irradiated in a.) FFTF at 407°C to 47 dpa and 5 at. ppm He and b.) HFIR at 400°C to 36.5 dpa and 30.5 at. ppm He

5. Microstructures of 9Cr-1MoVNb-2Ni irradiated in a.) FFTF at 407°C to 47 dpa and 5 at. ppm He and b.) HFIR at 400°C to 37.2 dpa and 402.5 at. ppm He. Higher magnification in kinematical contrast shows fine helium bubbles and larger voids.

6. Cavity size distribution histograms for various steels irradiated in HFIR, from quantitative analysis of low magnification photomicrographs which include the largest cavities (very fine bubbles would be obscure).

7. Cavity size distribution histograms from quantitative analysis of higher magnification photomicrographs which include the smallest visible helium bubbles.

8. Lower magnification TEM of 9Cr-1MoVNb-2Ni showing prior austenite grain size and lath packet and subgrain boundary structures in a.) as-tempered, and in b.) FFTF irradiated (407°C, 47 dpa, ~5 at. ppm. He) material.

9. Higher magnification TEM of 9Cr-1MoVNb-2Ni showing lath subgrain boundary and intra-lath dislocation structures in a.) as-tempered, and b.) FFTF irradiated (407°C, 47 dpa, ~5 at. ppm. He) material.

10. Higher magnification TEM of 12Cr-1MoVW showing lath subgrain boundary and intra-lath dislocation structures in a.) as-tempered, and b.) HFIR irradiated (400°C, 36 dpa, 85 at. ppm. He) material.

11. Higher magnification TEM of carbon film extraction replicas from 9Cr-1MoVNb a.) as-tempered, and b.) after HFIR irradiation at 400°C to 36.5 dpa and 30.5 at. ppm He. Changes (coarsening) of the MC precipitate structure after irradiation can be seen.

12. Histograms of MC phase composition (metallic elements) for quantitative XEDS analysis of precipitate particles extracted on replicas from as-tempered and from irradiated 9Cr-1MoVNb.

13. Histograms of MC phase composition (metallic elements) from quantitative XEDS analysis of precipitate particles extracted on replicas from irradiated 9Cr-1MoVNb.

14. Higher magnification TEM of fine M_6C (η) particles produced by irradiation of 9Cr-1MoVNb-2Ni irradiated in FFTF at 407°C to 47 dpa, a.) in-foil and b.) on a carbon film extraction replica.

15. Histograms of M_6C (η) phase composition (metallic elements) from quantitative XEDS analysis of precipitate particles extracted on replicas from irradiated 9Cr-1MoVNb-2Ni.

Table 1. Compositions of 9Cr-1MoVNb and 12Cr-1MoVW heats of steel with and without nickel doping

Alloy Designation	Heat No.	Concentration,[a] wt %										
		Cr	Mo	Ni	Mn	C	Si	V	Nb	Ti	W	N
9Cr-1MoVNb	(XA 3590)	8.6	1.0	0.1	0.36	0.09	0.08	0.21	0.063	0.002	0.01	0.05
9Cr-1MoVNb-2Ni	(XA 3591)	8.6	1.0	2.2	0.36	0.064	0.08	0.22	0.066	0.002	0.01	0.05
12Cr-1MoVW	(XAA 3587)	12	0.9	0.4	0.5	0.2	0.18	0.27	0.018	0.003	0.54	0.02
12Cr-1MoVW-2Ni	(XAA 3589)	11.7	1.0	2.3	0.5	0.2	0.14	0.31	0.015	0.003	0.54	0.02

[a]Balance iron.

Table 2. Normalizing and tempering conditions for various steels

Alloy	Normalization	Tempering
9Cr-1MoVNb	0.5 h at 1040°C	1 h at 760°C
9Cr-1MoVNb-2Ni	0.5 h at 1040°C	5 h at 700°C
12Cr-1MoVW	0.5 h at 1050°C	2.5 h at 780°C
12Cr-1MoVW-2Ni	0.5 h at 1050°C	5 h at 700°C

Table 3. Damage parameters and helium levels for nickel-doped and undoped 9Cr-1MoVNb and 12Cr-1MoVW steels irradiated in FFTF and HFIR

Alloy	Reactor	Irradiation Temperature (°C)	Displacement Damage (dpa)[a]	Helium Content (appm)
9Cr-1MoVNb	FFTF	407	47	~5
	HFIR	400	36.5	30.5
9Cr-1MoVNb-2Ni	FFTF	407	47	~5
	HFIR	400	37.2	402.5
12Cr-1MoVW	FFTF	407	47	~5
	HFIR	400	36.4	85.3
12Cr-1MoVW-2Ni	FFTF	407	47	~5
	HFIR	400	37.1	429.0

[a]dpa calculation includes the effect of nickel recoils.

Table 4. Quantitative cavity statistics determined via TEM for 9Cr and 12Cr steels irradiated in HFIR and FFTF

Alloy	Cavity Statistics (Average) Diameter (nm)	Cavity Statistics (Average) Density (m^{-3})	Comments	Total cvf Swelling (%)	Cavity Character Ratio
			FFTF Irradiation at 407°C to 47 dpa		
9Cr-1MoVNb			A few detectable voids (7–23 nm diam)		
9Cr-1MoVNb-2Ni			A few detectable voids (7–23 nm diam)		
12Cr-1MoVW			A few detectable voids (15–23 nm diam)		
12Cr-1MoVW-2Ni			A few detectable voids (15–23 nm diam)		
			HFIR Irradiation at 400°C to ~37 dpa		
9Cr-1MoVNb	9.2	2.71×10^{21}	Few fine cavities below ~3 nm diam, somewhat nonuniform spatial distribution. Many 10 to 20-nm-diam voids	~0.3	0.04
9Cr-1MoVNb-2Ni	3.8 12	1.6×10^{22} 2.5×10^{21}	Fine bubbles Larger voids	0.35	0.33
12Cr-1MoVW	12.5	2.2×10^{21}	Abundant fine cavities and a smaller population of larger voids. Critical size appears to be about ~5 nm (diam). Voids range up to 22 μm in diameter, but many are in the 10 to 15 μm range. Some fine cavities, but many 8 to 20 nm (diam) voids, with some in the 20 to 30 nm range in larger subgrains. Somewhat nonuniform distribution with most voids in largest subgrains, but all subgrains have some voids.	0.23	0.13
12Cr-1MoVW-2Ni	3.5 9	3.5×10^{22} 1.6×10^{21}	Fine bubbles Larger voids	0.25	0.45
			Abundant fine cavities and a sparse, nonuniform distribution of larger voids, many within larger subgrains.		

Table 5. Precipitate phase identification for 9Cr and 12Cr steels irradiated in HFIR and FFTF

Alloy	Phases after Tempering	Phases after Irradiation[a]		Comments
		HFIR (400°C, 37 dpa)	FFTF (407°C, 47 dpa)	
9Cr-1MoVNb	$M_{23}C_6$ (85%)[b] MC (15%)	$M_{23}C_6$ MC	$M_{23}C_6$ MC M_2X	Partial dissolution of coarse $M_{23}C_6$ particles and coarsening of finer MC particles. Traces of very fine M_2X acicular needles are found only in FFTF-irradiated material. MC composition is modified — more Cr, less V.
9Cr-1MoVNb-2Ni	$M_{23}C_6$ (85%)[b] MC (15%)	$M_{23}C_6$ M_6C (η) MC	$M_{23}C_6$ M_6C (η) MC M_2X	Some dissolution and coarsening of original as-tempered $M_{23}C_6$ particles and abundant precipitation of new $M_{23}C_6$ particles with slightly modified composition. MC evolution and modification are similar to that mentioned above. Many fine M_6C particles form in both reactors, but large M_6C particles are also found in FFTF-irradiated material. Some large M_2X particles are also found at boundaries in FFTF-irradiated material, but no fine needles.
12Cr-1MoVW	$M_{23}C_6$ (99%) MC (1%)	$M_{23}C_6$ M_6C (η)[c] MC	$M_{23}C_6$ M_6C (η)[c] MC	As-tempered $M_{23}C_6$ is stable while MC content increases during irradiation. MC composition is modified. Abundant, fine particles are found throughout the matrix, similar to M_6C mentioned above. In HFIR, these particles are very rich in Si and Cr, but in FFTF they have somewhat more Cr and less Si.
12Cr-1MoVW-2Ni	$M_{23}C_6$ (99%) M_6C (1%)	$M_{23}C_6$ M_6C (η) MC	$M_{23}C_6$ M_6C (η) MC	Partial dissolution of as-tempered $M_{23}C_6$ occurs and some coarse M_6C forms to replace it, more so in HFIR than in FFTF. Abundant, fine M_6C forms in both reactors and more MC develops during irradiation with the same compositional modifications mentioned above.

[a]XEDS analysis on extraction replicas plus some SAD and CBED analysis.
[b]Relative phase fractions determined via broad-beam XEDS measurements.
[c]Mainly Cr- and Si-rich.

Table 6. Quantitative XEDS compositional analysis of $M_{23}C_6$ particles extracted from 9Cr-1MoVNb-2Ni steel specimens

Phase Composition, at. %[a]									Number of Particles Analyzed	Comments
Si	Ti	V	Cr	Fe	Ni	W	Nb	Mo		
As-Tempered, 5 h at 700°C										
0.5	0.2	3.6	62	25.4	1.2	n.d.	0.8	6	6	Large, >350 nm diam
0.6	0.2	6.2	68	17.1	1.0	n.d.	0.4	6.2	3	Small, <150 nm diam
Irradiated in HFIR at 400°C to 37 dpa										
3.4	0.2	1.9	59	22.8	6.9	n.d.	0.2	5	2	Large, >350 nm in diam along boundaries
4.0	0.1	1.7	61	22.8	5.1	n.d.	0.2	4.4	2	Large, >200–500-nm-long laths in the matrix
Irradiated in FFTF at 407°C to 47 dpa										
3.4	0.2	1.5	60	20.9	6.8	n.d.	0.4	5.1	3	Large, >350 nm in diam along boundaries
2.0	0.2	0.8	63	24.8	2.9	n.d.	0.1	4.8	3	Large, >200–500-nm-long laths in the matrix

[a]Composition of metal atoms heavier than Al.

Table 7. Quantitative XEDS compositional analysis of MC particles extracted from 9 Cr steel specimens

Alloy	Phase Composition, at. %[a]									Number of Particles Analyzed	Comments[b]
	Si	Ti	V	Cr	Fe	Ni	W	Nb	Mo		
As-Tempered, 1 h at 760°C											
9Cr-1MoVNb	1.6	0.6	62.6	16.6	1.6	n.d.	n.d.	14.2	1.1	6	V-rich, small, 17–60 nm
	2.3	2.3	33	9.2	1.1	0.1	n.d.	49	1.3	2	Nb-rich, same
As-Tempered, 5 h at 700°C											
9Cr-1MoVNb-2Ni	0.3	0.6	69.2	14.0	0.8	n.d.	n.d.	14.0	0.8	7	V-rich, small, 17–60 nm
	1.3	2.1	26.5	5.3	0.8	n.d.	n.d.	62.4	0.5	2	Nb-rich, same
FFTF, 407°C, 47 dpa											
9Cr-1MoVNb	2.3	n.d.	33.7	52.7	4.8	0.5	n.d.	2.9	1.2	4	V-rich, larger, 70–150 nm
	2.8	0.1	35.1	49.4	6.5	0.4	n.d.	3.0	1.0	3	V-rich, smaller, 17–50 nm
	0.1	0.1	14.9	35.8	5.3	0.6	n.d.	40.3	1.1	4	Nb-rich, smaller
FFTF, 407°C, 47 dpa											
9Cr-1MoVNb-2Ni	4.4	0.2.	37.5	35.0	8.7	3.6	n.d.	7.4	1.5	4	V-rich, larger, >30 nm
	3.7	0.4	38.5	31.1	6.3	3.0	n.d.	13.2	1.3	3	V-rich, smaller, 9–25 nm
	3.2	1.1	9.8	21.6	5.0	6.2	n.d.	45.5	1.5	3	Nb-rich, larger, >90 nm
HFIR, 400°C, 36.5 dpa											
9Cr-1MoVNb	3.2	0.5	34.9	46.5	5.5	0.4	n.d.	7.4	1.4	9	V-rich, 30–120 nm
	0.4	1.2	8.8	34.2	4.5	0.8	n.d.	46.1	3.5	2	Nb-rich, same
HFIR, 400°C, 37 dpa											
9Cr-1MoVNb-2Ni	1.4	0.2	44.5	38.7	5.5	6.9	n.d.	5.6	1.4	4	V-rich, larger, 40–80 nm
	1.6	0.5	35.3	41.3	6.3	2.5	n.d.	9.6	1.6	4	V-rich, smaller, 8–25 nm

[a]Composition of metal atoms heavier than Al.
[b]Particle size, either diameter for equiaxed or larger dimension for other morphologies.

Table 8. Quantitative XEDS compositional analysis of fine $M_6C(\eta)$ particles extracted from 9 Cr and 12 Cr steel specimens

Alloy	Number of Particles Analyzed	Composition, at. %[a]								
		Si	Ti	V	Cr	Fe	Ni	W	Nb	Mo
		FFTF, 407°C, 47 dpa								
9Cr-1MoVNb-2Ni	9	15	0.1	0.4	36	13	29.2	n.d.	0.4	3.6
12Cr-1MoVW	3	18.4	1.1	0.7	64.2	7.3	1.0	1.2	0.2	2.9
12Cr-1MoVW-2Ni	6	12	0.1	2.6	38.5	13.5	25.1	1.0	1.0	5.5
		HFIR, 400°C, 37 dpa								
9Cr-1MoVNb-2Ni	4	14.7	0.1	0.6	40.1	13.7	25.3	n.d.	0.4	3.9
12Cr-1MoVW	5	25	0.8	6.2	48	7.0	2.1	0.7	4.6	2.4
12Cr-1MoVW-2Ni	7	15	0.7	2.4	40.3	12.7	25.4	0.6	0.3	1.7

[a]Composition of metal atoms heavier than aluminum.

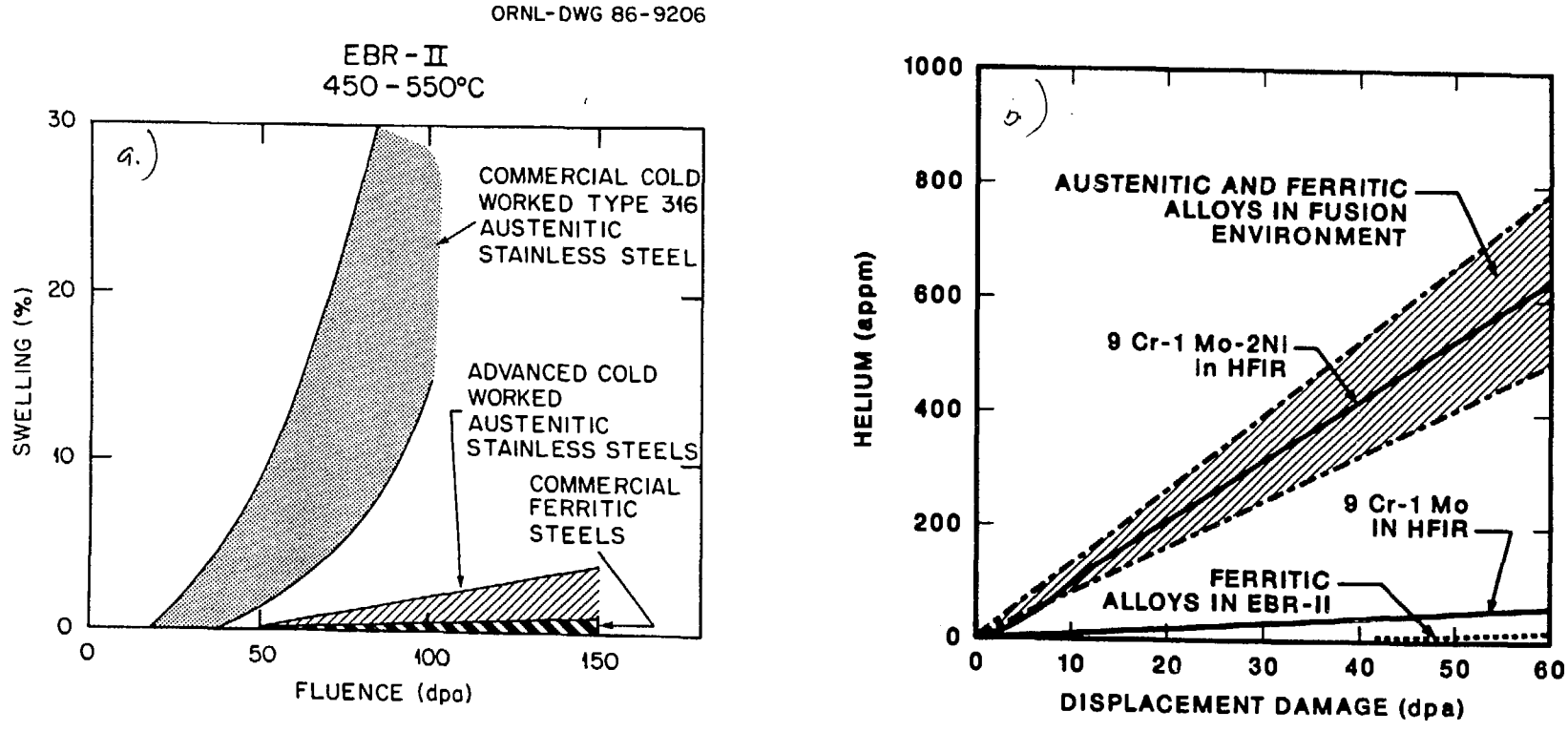
ORNL-DWG 86-9206
EBR-II
450-550°C
a.)
SWELLING (%)
30
20
10
0
0
50
100
150
FLUENCE (dpa)
COMMERCIAL COLD WORKED TYPE 316 AUSTENITIC STAINLESS STEEL
ADVANCED COLD WORKED AUSTENITIC STAINLESS STEELS
COMMERCIAL FERRITIC STEELS
b.)
HELIUM (appm)
1000
800
600
400
200
0
0
10
20
30
40
50
60
DISPLACEMENT DAMAGE (dpa)
AUSTENITIC AND FERRITIC ALLOYS IN FUSION ENVIRONMENT
9 Cr-1 Mo-2Ni In HFIR
9 Cr-1 Mo IN HFIR
FERRITIC ALLOYS IN EBR-II

Fig. 1

Ni-DOPING EFFECTS PRECIPITATION IN 9 Cr STEELS, BUT HELIUM CAUSES MORE VOIDS TO FORM IN HFIR

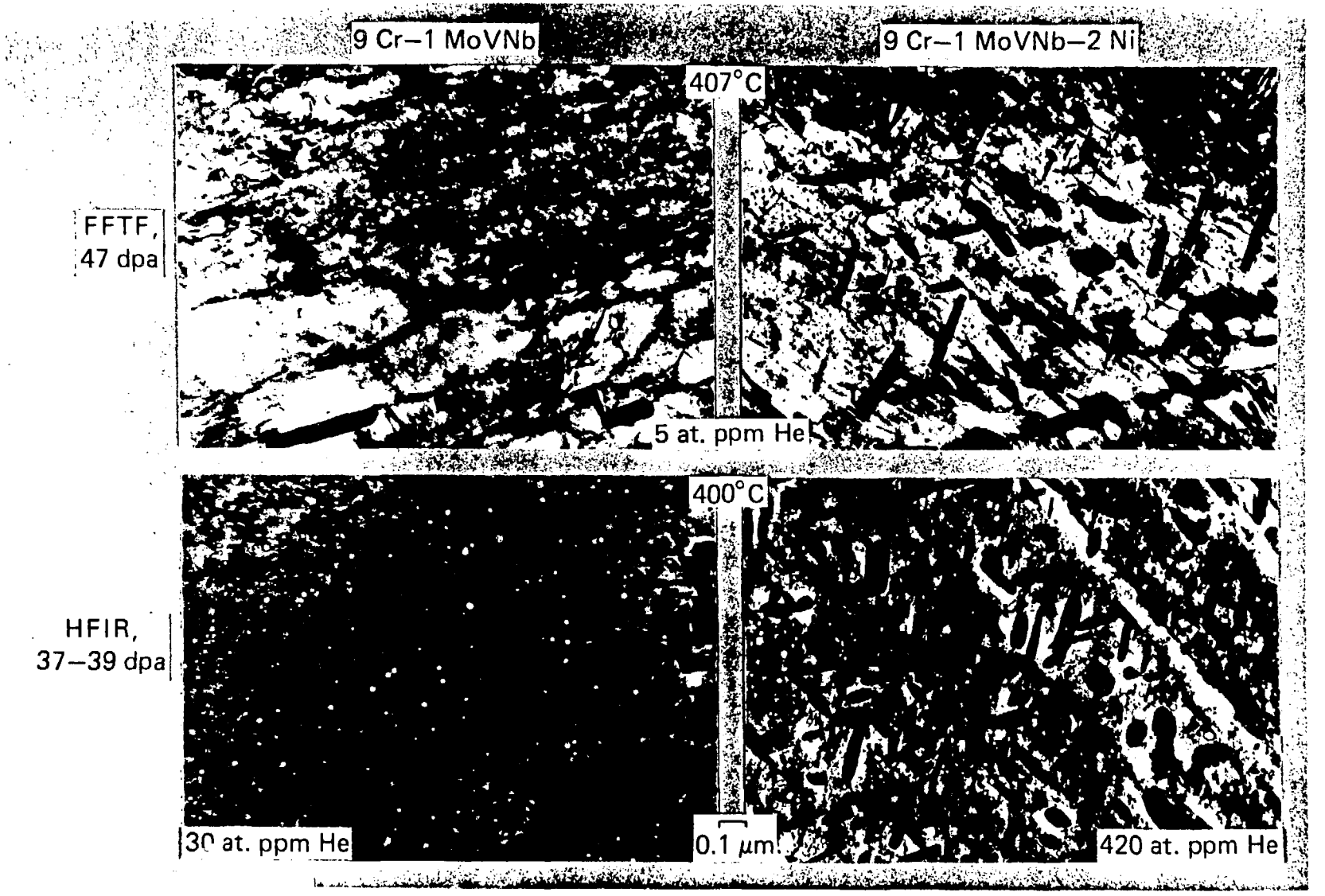

ornl

Ni-DOPING DOES NOT STRONGLY AFFECT PRECIPITATION OR VOID FORMATION IN HFIR IRRADIATED 12 Cr STEELS

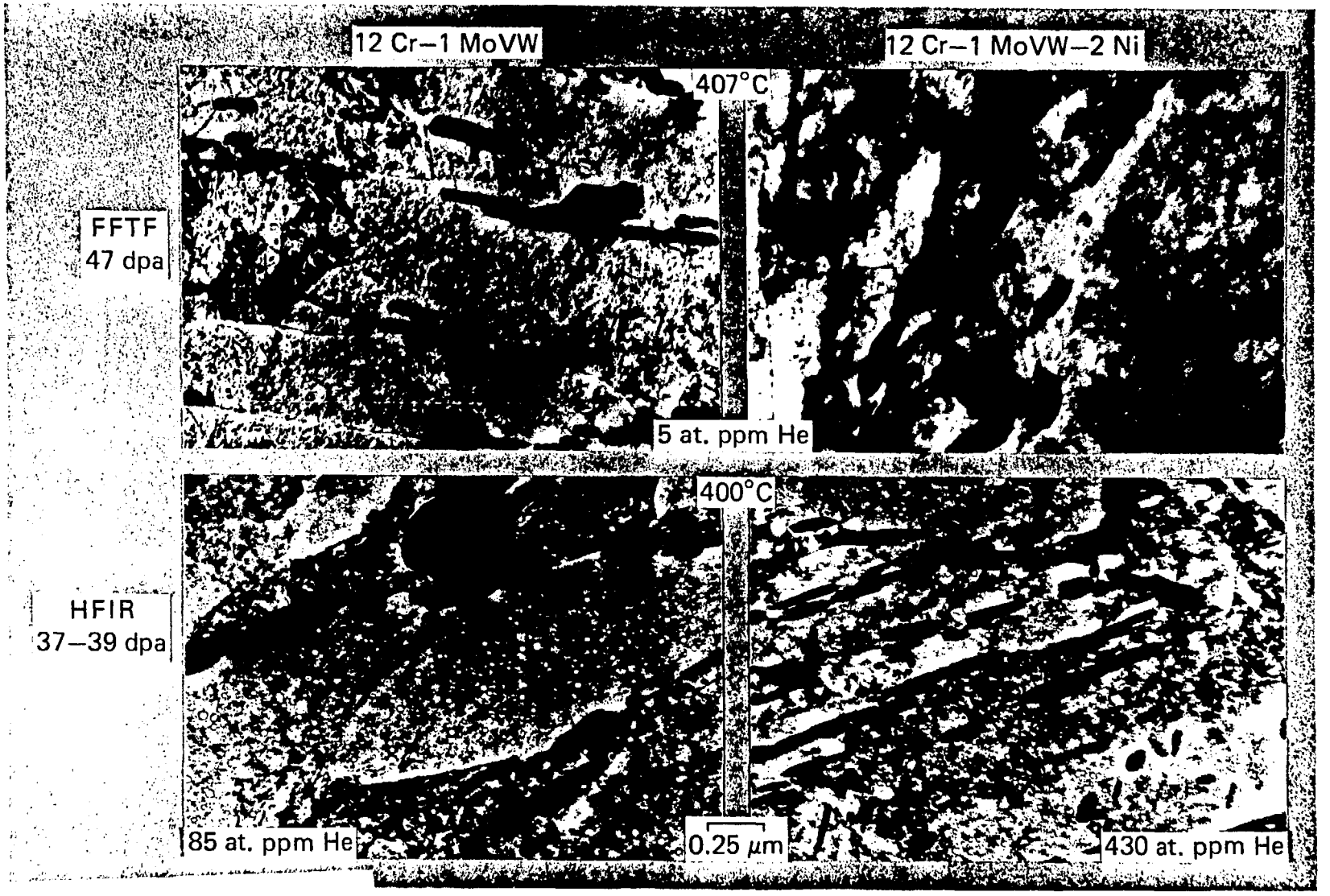

Fig. 3

ornl

Fig. 4a. 20 nm

Fig. 4b.

E 43222

YE 13012

Fig. 5a

20 nm

E 50252

YE 13767

Fig. 5b

E43133

YE 13311

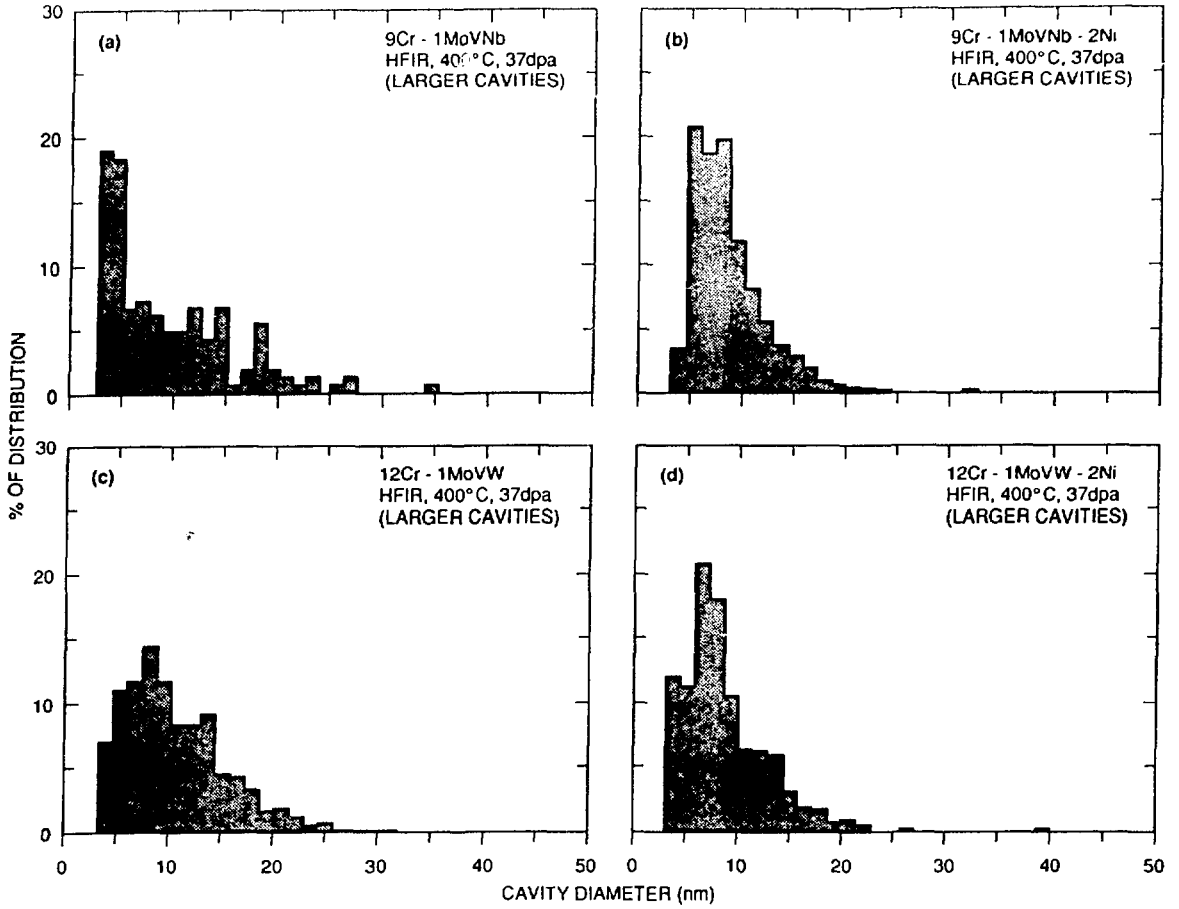
(a)
9Cr - 1MoVNb
HFIR, 400°C, 37dpa
(LARGER CAVITIES)
(b)
9Cr - 1MoVNb - 2Ni
HFIR, 400°C, 37dpa
(LARGER CAVITIES)
(c)
12Cr - 1MoVW
HFIR, 400°C, 37dpa
(LARGER CAVITIES)
(d)
12Cr - 1MoVW - 2Ni
HFIR, 400°C, 37dpa
(LARGER CAVITIES)
% OF DISTRIBUTION
CAVITY DIAMETER (nm)

Fig. 6

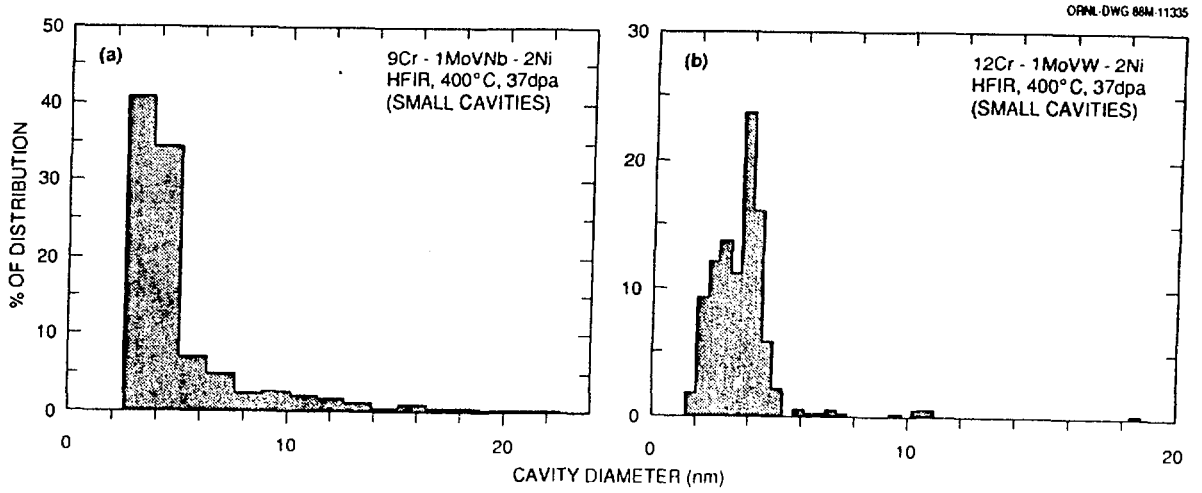
ORNL-DWG 88M-11335
(a)
9Cr - 1MoVNb - 2Ni
HFIR, 400°C, 37dpa
(SMALL CAVITIES)
(b)
12Cr - 1MoVW - 2Ni
HFIR, 400°C, 37dpa
(SMALL CAVITIES)
% OF DISTRIBUTION
CAVITY DIAMETER (nm)

Fig. 7

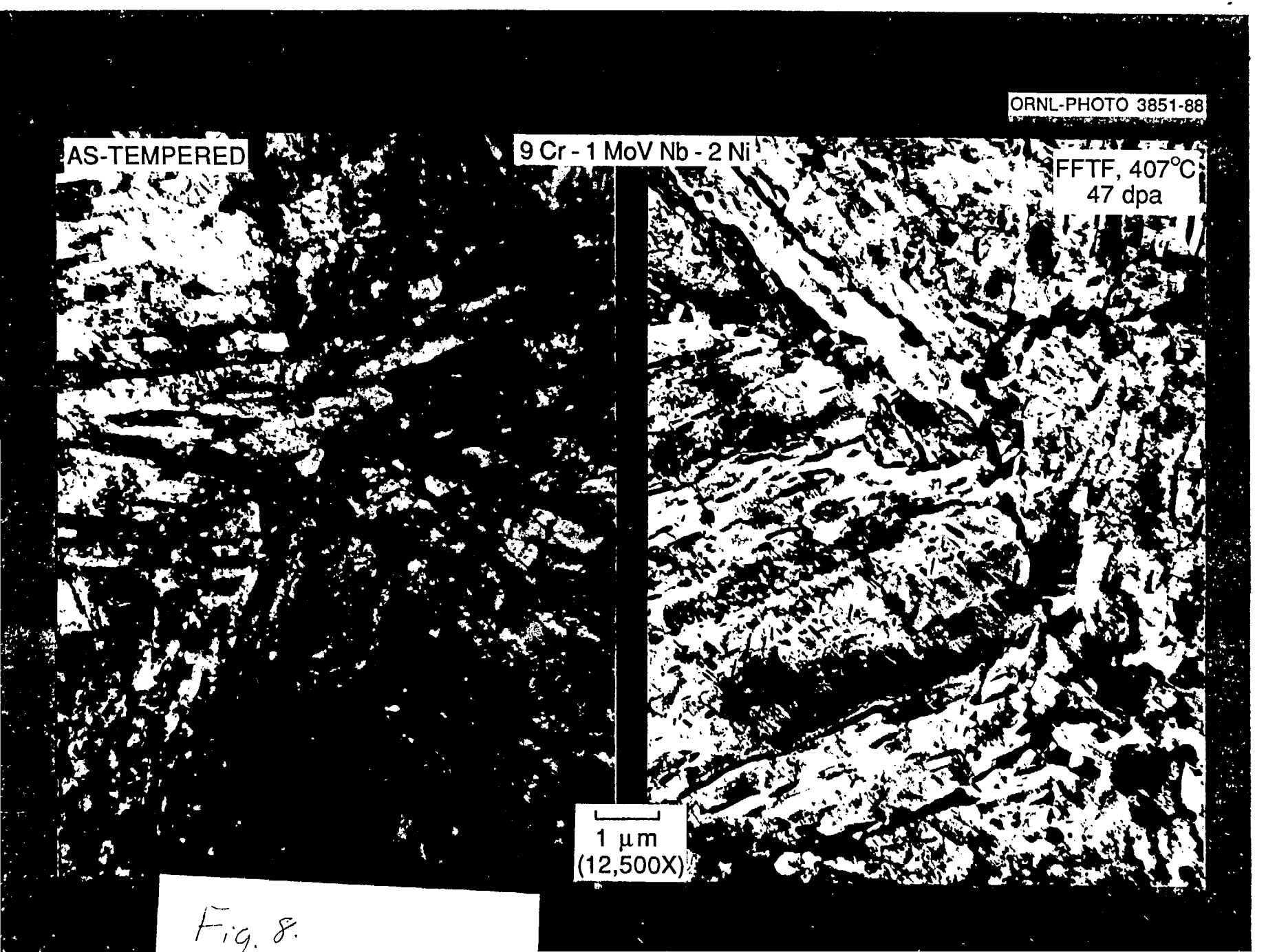
ORNL-PHOTO 3851-88
AS-TEMPERED
9 Cr - 1 MoV Nb - 2 Ni
FFTF, 407°C
47 dpa
1 µm
(12,500X)

Fig. 8.


ORNL-PHOTO 3854-88
AS-TEMPERED
9 Cr - 1 MoV Nb - 2 Ni
FFTF, 407°C
47 dpa
0.25 μ m
(65,200X)

Fig. 9

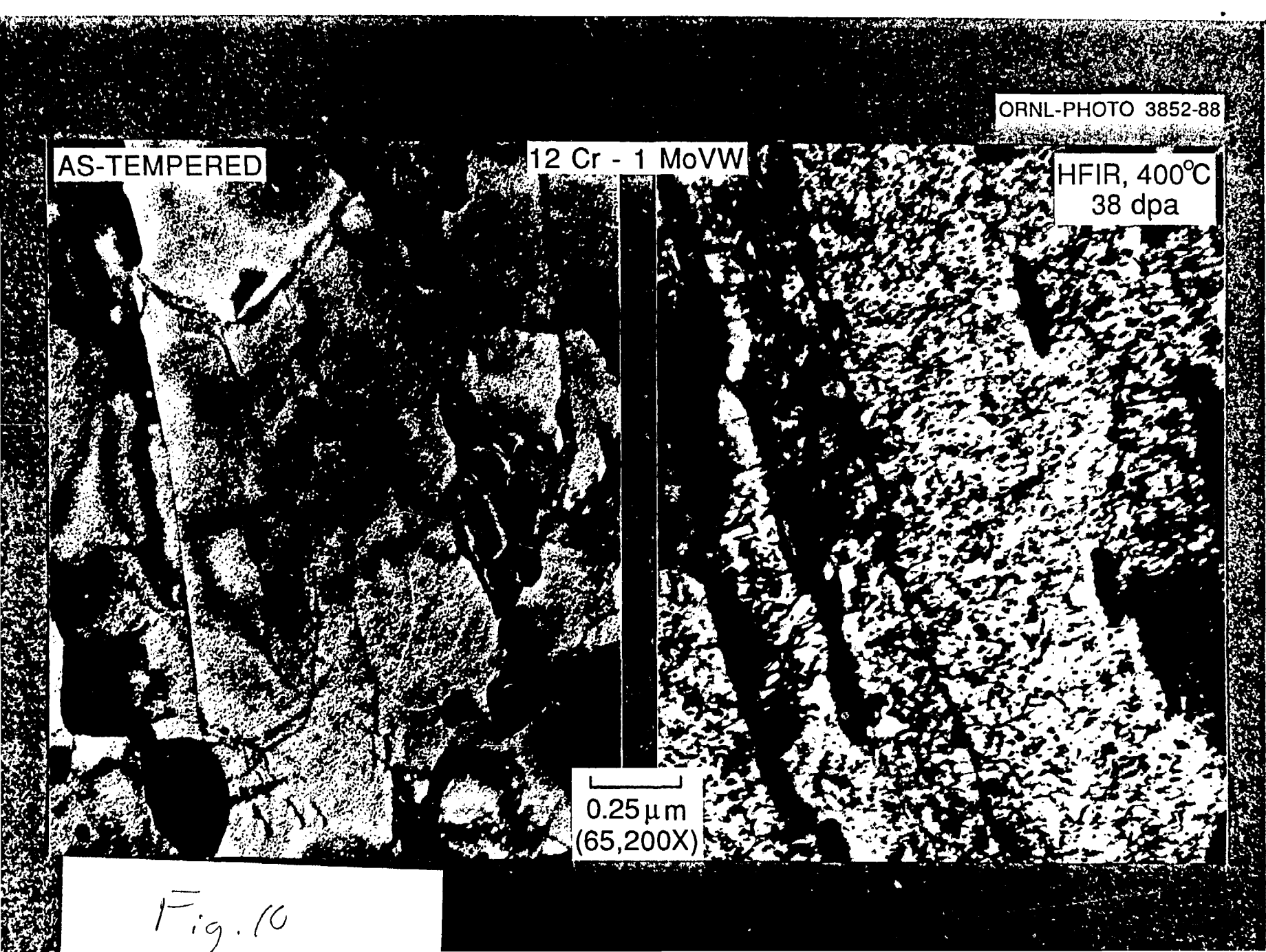
ORNL-PHOTO 3852-88
AS-TEMPERED
12 Cr - 1 MoVW
HFIR, 400°C
38 dpa
0.25 µm
(65,200X)

Fig. 10

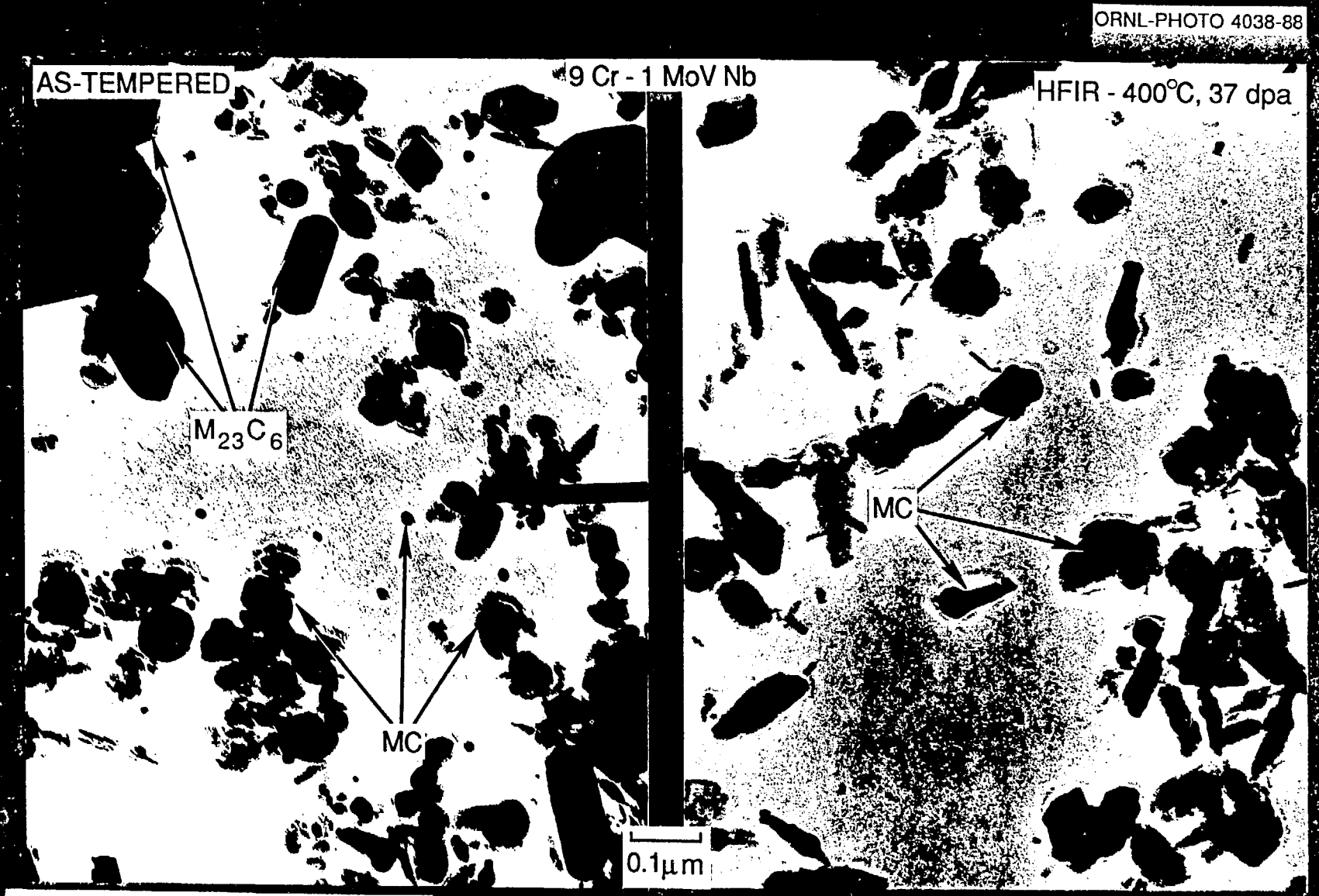
ORNL-PHOTO 4038-88
AS-TEMPERED
9 Cr - 1 MoV Nb
HFIR - 400°C, 37 dpa
$M_{23}C_6$
MC
MC
0.1μm

Fig. 11

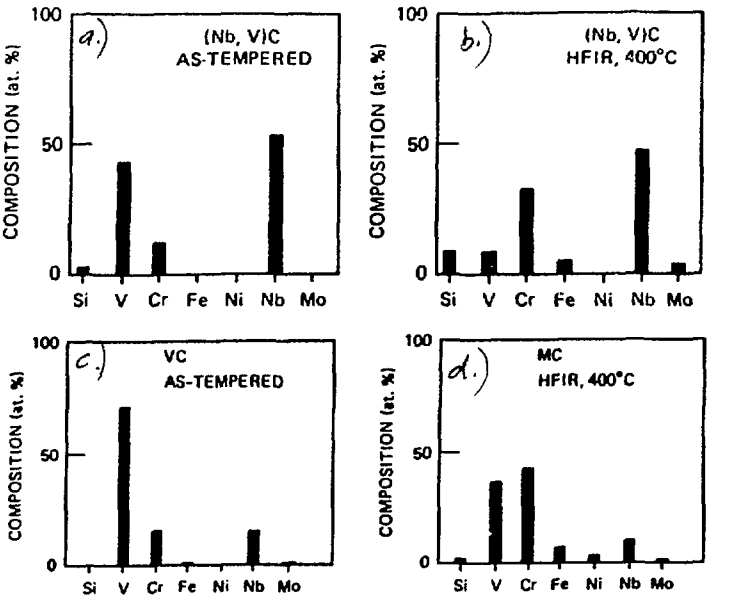

Fig. 12

ORNL-DWG 88-11181

9 Cr - 1 MoV Nb - 2 Ni

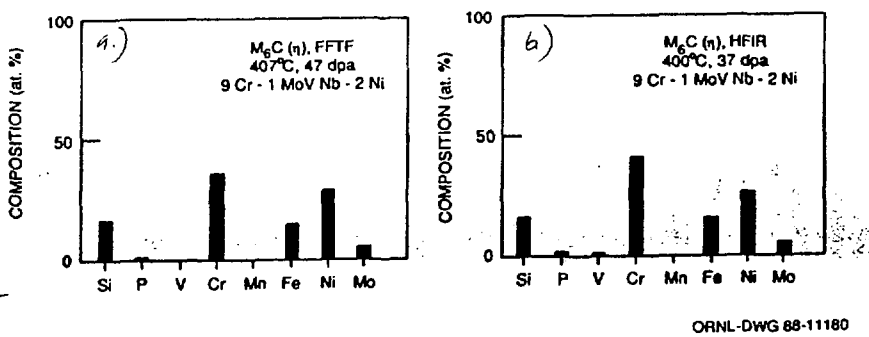

Fig. 15

ORNL-DWG 88-11180

9 Cr - 1 MoV Nb

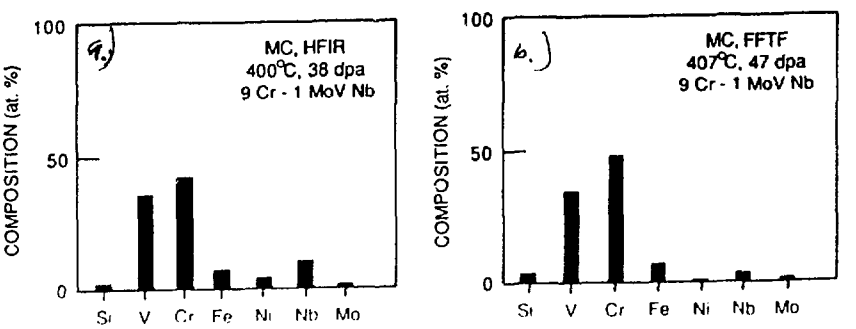

Fig. 13

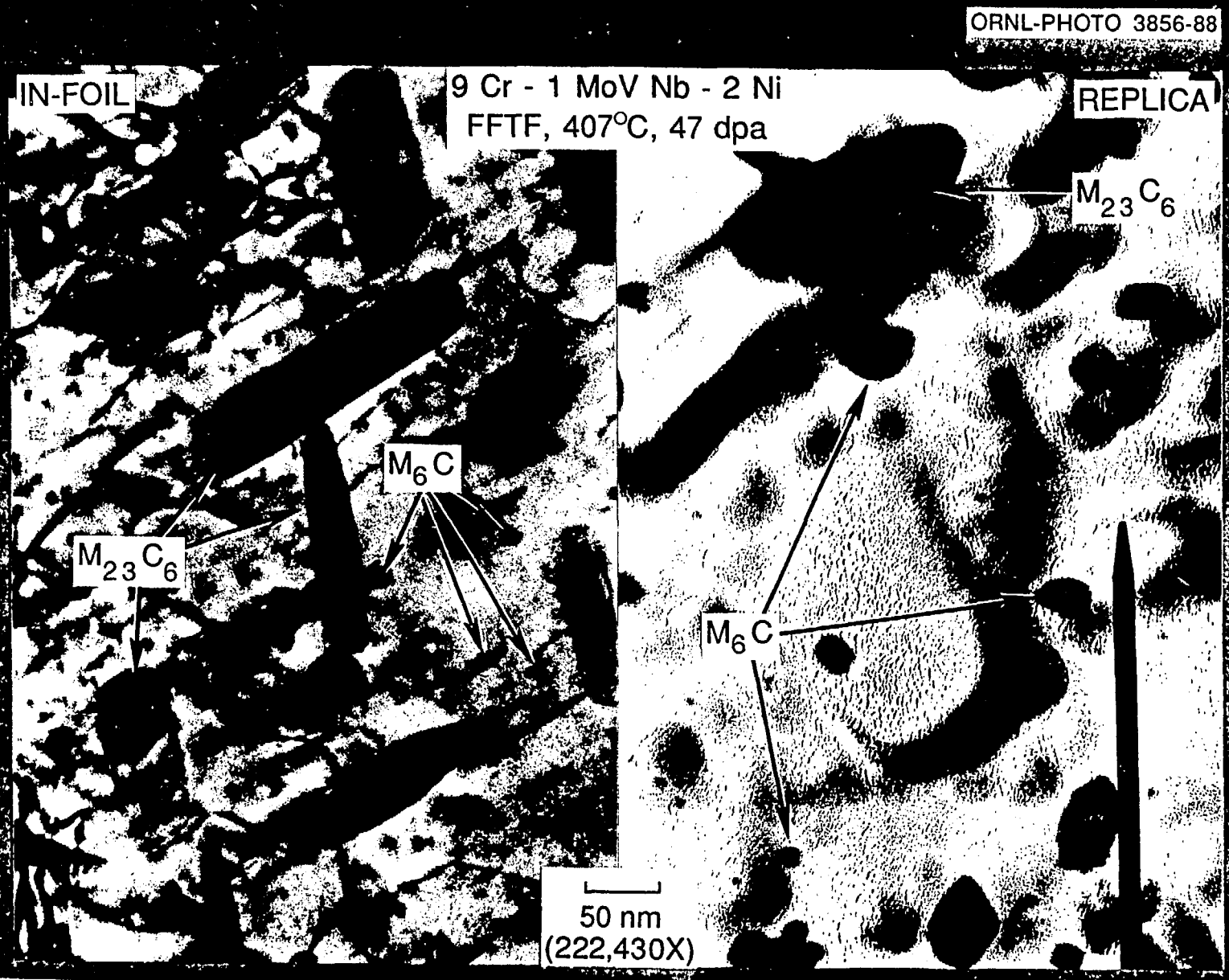
ORNL-PHOTO 3856-88
IN-FOIL
9 Cr - 1 MoV Nb - 2 Ni
FFTF, 407°C, 47 dpa
REPLICA
$M_{23}C_6$
M_6C
$M_{23}C_6$
M_6C
50 nm
(222,430X)

Fig. 14